SHIRSHOV INSTITUTE OF OCEANOLOGY

CRUISE REPORT No. 49

RV *AKADEMIK IOFFE* CRUISE 12 June – 5 July 2015

North Atlantic Repeat Hydrography of WOCE section along 59.5 N

Principal Scientist **S. Gladyshev**[1]

2016

Shirshov Institute of Oceanology
36 Nakhimovskii prospect
Moscow 117997 RUSSIA
Tel: +7(495) 719 0255 Fax: +7(499) 124 6342 Email:

sgladyshev@ocean.ru

[1]**Shirshov Institute of Oceanology**

DOCUMENT DATA SHEET

AUTHOR	***PUBLICATION DATE***
GLADYSHEV, S	2016

TITLE

RV ***Akademik Ioffe*** Cruise 49 , 12 June – 5 July 2016.

REFERENCE

Shirshov Institute of Oceanology, Akademik Ioffe Cruise Report, No. 49, 70pp. tables & figs.

ABSTRACT

RV ***Akademik Ioffe*** Cruise 49 was a contribution to the Russian CLIVAR and WORLD OCEAN Research Programmes. CTD section was designed to enable the ocean circulation in the Subpolar gyre of the North Atlantic to be mapped and in particular the course of the North Atlantic, Irminger and East Greenland Currents within the region to be determined. The main goal is to continue annual monitoring of the North Atlantic large-scale circulation and climate changes in the North Atlantic.

12 stations (3403-3414) were made at the Greenland shelf and continental slope to determine the coastal East Greenland Current.

KEYWORDS

CRUISE 49 2015, *AKADEMIK IOFFE,* **CLIVAR, TRANSATLANTIC SECTION, EAST GREENLAND CURRENT, IRMINGER BASIN, NORTH ATLANTIC SUBPOLAR GYRE, CLIVAR, CTD OBSERVATIONS, LADCP, VMADCP**

ISSUING ORGANISATION

Shirshov Institute of Oceanology
36 Nakhimovskii prospect
Moscow 117997 RUSSIA

Director: Academician Robert Nigmatulin

Copies of this report are available from: **Department of Marine Operations,** Tel: +7(495)7190255 Fax: +7(499)124 6342

Email: sgladyshev**@ocean.ru**

Contents

Scientific Personnel

GLADYSHEV, S.	Principal Scientist	Shirshov
PYATAKOV, V.	Chief of CTD group	Shirshov Atlantic Branch
GLADYSHEV, V.	CTD, LADCP, Sampling	Shirshov
ZAPOTYL'KO, V.	CTD, LADCP	Shirshov
AGARKOV, A.	CTD, LADCP, Sampling	Shirshov
KULESHOV, A.	Winch	Shirshov Atlantic Branch
LUKASHIN, S.	Winch, Sampling	Shirshov Atlantic Branch
MARKINA, M	Meteo observations	Shirshov
BULYCHEV, V.	Oxygen	Shirshov Atlantic Branch
STEPANOVA, S.	Nutrients	Shirshov
KOLOKOLOVA, A.	Chief of Chemistry group	Shirshov
MUSTAEVA V.	Nutrients	Shirshov Atlantic Branch
DEMIDOV, A.	Primary Production, Chl	Shirshov
MOSHAROV, S.	Primary Production, Chl	Shirshov
GAGARIN, V	Primary Production, Chl	Shirshov
KRINITSKII, M.	Meteo observations	Shirshov
GAVRIKOV, A.	CTD, LADCP, Sampling	Shirshov
KLYUVITKIN, A.	Ghief of geological group	Shirshov
POLITOVA, N.	Suspended Sediment matter	Shirshov
NOVICHKOVA, E.	Bottom sediment treatment	Shirshov
NOVIGATSKII A.	Gravity Corer, moorings	Shirshov
KOZINA, N.	Bottom sediment treatment	Shirshov
BUDKO, D.	Grab Sampler, moorings	Shirshov
SAVVICHEV, A.	Microbiology	Shirshov
ISACHENKO, S.	Geological Winch	Shirshov
AMBROSIMOV, A.	Gravity Corer, moorings	Shirshov
BASHIROVA, L.	Bottom sediment treatment	Shirshov
STUDHOLME, J.	Sampling	Shirshov
BOUDREAU, D.	Sampling	Dalhousie University (Canada)

1. CRUISE NARRATIVE

1.1 Cruise Details

Expedition Designation: R/V ***Akademik Ioffe*** Cruise 49, RUSSIA CLIVAR

Principal Scientist: Dr. Sergey V. Gladyshev (Shirshov).

Ship: RV ***Akademik Ioffe.***

Ports of Call: Gdansk (Poland) to Halifax (Canada).

Cruise Dates: 12th June to 5th July 2015.

1.2 Cruise Summary

1.2.1 Cruise Track and Stations

The cruise track with station positions is shown in **Fig. l**. Only small volume samples were taken, details are listed in **Table 1**.

1.2.2. Equipment

The principal instruments used during the cruise were a SBE 9P-743 CTD with dual temperature and conductivity sensors (SBE 3 SN 03P5677, SBE 4 SN 042827, SBE 3 SN 03P4401, SBE 4 SN 042925), oxygen sensor (SBE 43, SN 430699), turbidity sensor (SeaPoint Turbidity, SN 10218 STM), Benthos altimeter model PSA-900D, LADCP WHS-300 kHz down-looking (S/N 6393), LADCP WHS-300 kHz up-looking (S/N 14151). These were mounted together with a multisampler Carousel SBE 32 equipped with 22 5-litre Niskin bottles. Upon recovery each bottle was sampled in turn for dissolved oxygen, nutrients, salinity. All sampling was done on deck. Currents were measured using vessel mounted ADCP (VMADCP) TRDI OS38 kHz (S/N 1185) installed at the central point of the ship hall.

Navigation information was provided by a Trimble SPSx50/SPSx51 - Modular GPS receiver and every second was recorded on the PC. Additional measurements were made with an ELAC 12 kHz, Aanderaa meteorological package.

1.2.3 Sampling

Nominal depths sampled were: bottom, 3100, 3000, 2750, 2500, 2250, 2000, 1750, 1500, 1250, 1100, 1000, 900, 800, 700, 600, 500, 400, 300, 200, 150, 100, 50, 30, 20, 10 m. On deep casts fewer shallow and intermediate bottles were fired. The actual bottle depths are shown in **Fig. 2**.

1.2.4 Number of Stations Occupied

86 stations (91 casts) were occupied during the cruise along transatlantic section along 59.5 N (**Fig. l**).

1.3 Scientific Objectives

The cruise objectives were to:

1. To complete a CTD section from the Great Britain to Greenland.
2. To survey the North Atlantic Subpolar Gyre with high-resolution CTD and LADCP/VMADCP data to determine the circulation and meridional fluxes.

1.4 Narrative

1.4.1 Introduction

The Meridional overturning circulation (MOC) in the North Atlantic is one of the main drivers of the widely known global oceanic "conveyor belt" – an important element of the Earth's climate system [e.g., van Aken, 2007]. Warm upper-ocean waters transported northward by the North Atlantic Current release heat to the atmosphere, gain density due to cooling and eventually sink in the subpolar North Atlantic and adjacent Arctic seas thereby generating the return southward flow of colder waters at depths (**Fig. 3**) [Dickson and Brown, 1994; Koltermann et al., 1999]. Temporal variability of the large-scale circulation and associated heat transport in the subpolar North Atlantic is one of the principal factors behind the high-latitude climate anomalies in the Northern Hemisphere.

Progress in understanding the causes of the ongoing climate change and forecasting climate variability in the Arctic and over European part of Russia for the next decades require reliable observation-based estimates of the variability of the North Atlantic circulation and the Atlantic–Arctic heat and freshwater fluxes, as well as elucidation of the underlying mechanisms.

In a number of recent studies, radical changes in the thermohaline regime and large-scale circulation in the Atlantic Ocean have been suggested to occur under global warming. For instance, the long-term freshening of the subpolar North Atlantic deep waters since the mid-1960s [Dickson et al., 2002] has been (cautiously) attributed to climate change-related factors [Curry et al., 2003; Hansen et al., 2004]. Hypothetically, under global warming, an increased evaporation in the tropics and increased precipitation at high latitudes, coupled with an intensified melting of Arctic ice, lead to the upper-ocean freshening in the regions of deep water formation and, hence, to the deep water freshening in the Atlantic Ocean. At the same time, milder winters along with the upper-ocean freshening lead to a decrease in the deep water production rates, which results in slowing of the Atlantic Meridional Overturning Circulation [e.g., Hansen et al., 2004; Bryden et al., 2005].

To better understand the past and present changes in the ocean-atmosphere dynamical system, as well as their causes and consequences, data on the full-depth oceanic variability are needed. An indispensable effective tool for assessing the large-scale circulation and thermohaline changes in the deep ocean and investigating mechanisms governing these changes are repeated full-depth transoceanic observations.

Since 1997, the P.P. Shirshov Institute of Oceanology has carried out the long-term monitoring of the North Atlantic circulation and water mass properties in the 59.5°N hydrographic section between Cape Farewell (Greenland) and Scotland (**Fig. 3**). Since 2002, the section has been repeated yearly on board the Russian research vessels, providing high precision data on temperature, salinity, oxygen and nutrients concentrations, and current velocities in the entire water column – "from shore to shore", from the sea surface to the bottom. In 2011, in addition to annual repeat measurements at 59.5°N, the P.P. Shirshov Institute of Oceanology started full-depth repeat observations of the oceanic exchange between the Atlantic and Arctic oceans through the straits between Greenland, Iceland, Faeroe and Shetland Islands (**Fig. 3**). The full-depth observations – of the same oceanic quantities as at 59.5°N – are performed in the straits from research vessels twice a year, in summer and fall. Based on the unique data set thus collected, a number of fundamental findings have already been achieved. Below, we briefly summarize the main subjects and results of our research.

The 59.5°N transatlantic section (**Fig. 3**) was designed for monitoring the large-scale circulation and thermohaline / chemical properties of oceanic waters at the northern periphery of

the NA – the region where the warm upper-ocean waters are transformed by deep convection and mixing into the colder intermediate and deep waters – the Labrador Sea Water (LSW), Iceland Scotland Overflow Water (ISOW) and Denmark Strait Overflow Water (DSOW) (**Fig. 3**) – transported southward in the lower limb of the Atlantic MOC. Hydrographic data collected at 59.5°N along with those obtained within the framework of the kindred projects, primarily the French OVIDE (http://www.ifremer.fr/lpo/ovide), and historical data sets have been used for studying the dense water production [Falina et al., 2007; Falina et al., 2012], decadal temperature and salinity changes in the intermediate–deep water column [Sarafanov et al., 2007; Sarafanov et al., 2008; Sarafanov et al., 2010b], causes of these changes [Sarafanov, 2009; Sarafanov et al., 2010b], the mean state [Sarafanov et al, 2012] and long-term variability of the large-scale circulation in the region [Sarafanov et al., 2009; Sarafanov et al, 2010a; Våge et al., 2011].

1.4.2 Deep convection in the Irminger Sea

The oxygen data collected in 1997 in the northern North Atlantic in several sections ending nearby the southern tip of Greenland provided the observation-based support for the hypothesis [Pickart et al., 2003] that winter convection in the Irminger Sea may penetrate deep into the LSW layer (1000 – 2000 m) thus causing local renewal of this water mass. A separate lateral maximum of oxygen concentrations in the deep LSW layer was detected east of Cape Farewell (59.5°N, 36–40°W): the concentrations increased (by ~0.1 ml/l) from the Labrador Sea eastern edge toward the Irminger Sea (**Fig. 4**) rather than the reverse, as would be expected if LSW observed in the Irminger Sea interior in 1997 were solely of advective origin [Falina et al., 2007].

1.4.3. Reversal of the deep-water freshening

The LSW and Nordic Seas overflow-derived deep waters, ISOW and DSOW, freshened in the northern North Atlantic during the last three–four decades of the 20th century [Dickson et al., 2002]. Between the 1960s and 1990s, the water column in the region freshened on average by about 0.03 [Curry et al., 2003].

The long-term freshening reversed in the mid-1990s [Sarafanov et al., 2007; Sarafanov et al., 2008; Sarafanov et al., 2010b]. The salinification (and warming) of the intermediate and deep waters since the mid-1990s (**Fig. 5**) was much more intense than the preceding freshening. Over

nearly a decade (1997–2006), temperature / salinity in the intermediate–deep water column ($\sigma_0 \geq 27.45$, depths > 500–1000 m) at 59.5°N increased by ~0.3°C / 0.03–0.04 [Sarafanov et al., 2008].

In the Irminger Sea, the long-term freshening in the deep water column (σ_0>27.80, depths > ~2000 m) reversed in the early 2000s [Sarafanov et al., 2010b]. The observed freshening reversal was a lagged consequence of the persistent ISOW salinification that occurred upstream, in the Iceland Basin, after 1996 due to salinification of the northeast Atlantic waters entrained into the overflow. It was demonstrated [Sarafanov et al., 2010b] that the entrainment salinity increase was associated with the North Atlantic Oscillation (NAO)-induced weakening and contraction of the Subpolar Gyre and corresponding northwestward advance of subtropical waters that followed the NAO decline in the mid-1990s and continued through the mid-2000s. Remarkably, the deep water freshening reversal was not related to changes in the overflow water salinity.

1.4.4. Deep-ocean salinity changes and the NAO

Close relationship between the thermohaline properties of the northern North Atlantic intermediate and deep waters and the winter NAO index on a decadal time scale ($r^2 \approx 0.65$, 1950s–2000s, **Fig. 6b** and **6c**) was revealed [Sarafanov, 2009] from the observation-based salinity time series for LSW in the Labrador Sea [Yashayaev, 2007] and ISOW in the Iceland basin [Boessenkool et al., 2007; Sarafanov et al., 2007]. Persistent NAO decline (amplification) leads to warming and salinification (cooling and freshening) in the intermediate–deep water column.

An explanation for the close link between the NAO and the coherent decadal changes in the intermediate and deep water properties in the region was proposed [Sarafanov, 2009]. The two factors dominate this link (**Fig. 6d**): (i) intensity of convection in the Labrador Sea controlling injection of relatively cold fresh waters into the intermediate layer and (ii) zonal extent of the Subpolar Gyre that regulates the relative contributions of cold fresh subpolar waters and warm saline subtropical waters to the entrainment into the Norwegian Sea overflow south of the Iceland–Scotland Ridge and to the Atlantic inflow to the Nordic Seas. These factors act in

phase leading to the observed coherent thermohaline changes in the intermediate–deep water column.

Due to weakening of the surface forcing associated with the NAO transition into neutral to low phase (1950s to mid-1960s, mid-1990s to mid-2000s), convection in the Labrador Sea weakens diminishing cold fresh water penetration into the intermediate layer. This results in warming and salinification at the intermediate depths in the Subpolar Gyre. Concurrently, the Subpolar Gyre contracts allowing northward advance of warm saline upper-ocean and intermediate subtropical waters in the northeastern North Atlantic. Northward progression of subtropical waters increases temperature and salinity at the upper intermediate levels and, correspondingly, increases temperature and salinity of the northeast Atlantic waters entrained into the Iceland–Scotland overflow along its pathway to the deep Iceland basin. As a result, temperature and salinity at the deep levels increase. The contrary changes – intensification of deep convection in the Labrador Sea and expansion of the Subpolar Gyre – caused by amplifying surface forcing (mid-1960s to mid-1990s) lead to cooling and freshening at the intermediate–deep levels. Additionally, under high-NAO conditions, deep convection may occur in the Irminger Sea potentially contributing to cooling and freshening at the intermediate (LSW) levels. The two regimes of convection and large-scale circulation corresponding to stronger (early 1990s) and weaker (mid-1960s, mid-2000s) NAO-related atmospheric forcing are schematically visualized in **Fig. 7**.

1.4.5 Deep-ocean salinity changes and climate change

There are increasing concerns that in the warmer climate, the MOC may substantially decline due to a decrease in the convective activity in the northern North Atlantic and Nordic Seas [e.g., Meehl et al., 2007]. The long-term freshening in the Nordic Seas and freshening of the northern North Atlantic deep waters in the 1960s–1990s have been considered as a likely indicator or precursor of the dramatic change in the MOC [e.g., Hansen et al., 2004]. The freshening has been attributed to a combination of factors potentially associated with the global warming: the increasing ice melt and net precipitation at high latitudes [e.g., Curry et al., 2003]. A probable causality between the climate change and the decreasing North Atlantic deep water salinity has supported the concerns and unfavorable predictions, thus ‘warming up’ the reasonable scientific debate on climate change and overblown speculations in media.

Despite the long-term increase in freshwater input to the Arctic, freshening in the northern North Atlantic had reversed in the mid-1990s, as we demonstrated above. This reversal forces us to revise the hypotheses on the mechanisms behind the deep-water thermohaline anomalies. It seems doubtful that the persistent global temperature growth may lead to the opposite decadal trends (positive-then-negative-then-positive, **Fig. 6**) in the deep water salinity.

Our results [Sarafanov et al., 2008; Sarafanov, 2009; Sarafanov et al., 2010b] suggest that natural atmospheric variability over the North Atlantic plays the major role in the deep-water thermohaline variability on a decadal time scale. There are no reasons to associate the deep-water freshening in the 1960s–1990s with climate change, unless the 3-decade-long surface forcing amplification is evidently shown to be a consequence of the latter. Having said that, the net 1950s–2000s trends in the water mass salinities are negative implying that the global factors (e.g., probable intensification of hydrological cycle [Curry et al., 2003]) may act on longer time scales.

1.4.6 Decadal variability of the Deep Western Boundary Current at Cape Farewell

Recent decadal changes in the Deep Western Boundary Current (DWBC) transport southeast of Cape Farewell were assessed from hydrographic data (1991–2007, **Fig. 7a**), direct velocity measurements (2002–2006) and satellite altimetry (1992–2007). Following the approach used in earlier studies [e.g., Bacon, 1998], we first determined that the DWBC (σ_0>27.80) baroclinic transport (T_{BC}) referenced to 1000 m depth increased by ~2 Sv between the mid-1990s (1994–1997) and 2000s (2000–2007) (**Fig. 8b**) [Sarafanov et al., 2009]. In the next step, we quantified velocity changes at the reference level (1000 m) by combining estimates of the hydrography-derived velocity changes in the water column and the altimetry-derived velocity changes at the sea surface [see Sarafanov et al., 2010a]. The inferred increase in the southward velocity at 1000 m above the DWBC in 1994–2007 indicates that the increase in the DWBC absolute transport was larger but very close to the 2-Sv increase in the DWBC T_{BC}. This result along with the observed coherence of the DWBC absolute and baroclinic transport changes between individual observations [Sarafanov et al., 2010a] imply that the DWBC absolute transport variability in the region is well represented by its baroclinic component on decadal and shorter time scales.

The historical record of the DWBC T_{BC} (1955–2007, **Fig. 8c**) updated after Bacon [1998] shows distinct decadal variability (±2–2.5 Sv) with the transport minima in the 1950s and mid-1990s, maximum in the early 1980s and moderate-to-high transport in the 2000s. The DWBC T_{BC} decadal variability is consistent with the general pattern of the recent decadal hydrographic and circulation changes in the northern North Atlantic. The DWBC T_{BC} anomalies negatively correlate (R = –0.80, 1955–2007) with thickness anomalies of the Labrador Sea Water (LSW) at its origin implying a close link between the DWBC transport southeast of Cape Farewell and the LSW production in the Labrador Sea (**Fig. 8d**). During the recent three decades (late 1970s – late 2000s), the DWBC T_{BC} changes were also in-phase with changes in the strength and zonal extent of the Subpolar Gyre [see Sarafanov et al., 2010a]. In particular, the Gyre weakening at shallow levels in the mid-1990s – mid-2000s was accompanied by the DWBC strengthening in the Irminger Sea [Sarafanov et al., 2009; Sarafanov et al., 2010a; Våge et al., 2011]. The results imply that the decadal changes in the (i) LSW production, (ii) SPG strength and (iii) DWBC transport in the Irminger Sea are linked, representing a complex coherent oceanic response to the decadal variability of the surface forcing.

1.4.7 Mean state of the full-depth circulation in the 2000s

A mean state of the full-depth summer circulation in the Atlantic Ocean in the region in between Cape Farewell (Greenland), Scotland and the Greenland-Scotland Ridge (see **Fig. 3**) was assessed by combining 2002–2008 yearly hydrographic measurements at 59.5°N, mean dynamic topography, satellite altimetry data and available estimates of the Atlantic–Nordic Seas exchange [see Sarafanov et al., 2012]. The mean absolute transports by the upper-ocean, mid-depth and deep currents and the MOC (MOCσ=16.5±2.2 Sv, at σ_0=27.55) at 59.5°N were quantified in the density space. Inter-basin and diapycnal volume fluxes in between the 59.5°N section and the Greenland-Scotland Ridge were then estimated from a box model.

The estimated meridional and diapycnal volume fluxes contributing to the MOC are schematically visualized in **Fig. 9**. The dominant components of the meridional exchange across 59.5°N are the North Atlantic Current (NAC, 15.5±0.8 Sv, σ_0<27.55) east of the Reykjanes Ridge, the northward Irminger Current (IC, 12.0±3.0 Sv) and southward Western Boundary Current (WBC, 32.1±5.9 Sv) in the Irminger Sea and the deep water export from the northern Iceland Basin (3.7±0.8 Sv, σ_0>27.80). About 60% (12.7±1.4 Sv) of waters carried in the MOCσ

upper limb (σ_0<27.55) by the NAC/IC across 59.5°N (21.1±1.0 Sv) recirculates westwards south of the Greenland-Scotland Ridge and feeds the WBC. 80% (10.2±1.7 Sv) of the recirculating NAC/IC-derived upper-ocean waters gains density of σ_0>27.55 and contributes to the MOCσ lower limb. Accordingly, the contribution of light-to-dense water conversion south of the Greenland-Scotland Ridge (~10 Sv) to the MOCσ lower limb at 59.5°N is one and a half times larger than the contribution of dense water production in the Nordic Seas (~6 Sv).

1.4.8 Cascading of dense shelf waters in the Irminger Sea

Based on the hydrographic data collected at 59.5°N, 64.3°N and 65–66°N in the western Irminger Sea in the 1990s – 2000s, an observational evidence for the deep-reaching cascading of dense shelf waters south of the Denmark Strait was found [Falina et al., 2012]. The data collected in the northwestern Irminger Sea (65–66°N) indicate that the East Greenland Current ~200 km south of the Denmark Strait occasionally carries shelf waters as dense as the overflow-derived deep waters transported by the DWBC (σ_0 > 27.80). Hydrographic traces of cascading of dense shelf waters down the East Greenland slope were found from repeat measurements at 64.3ºN, where the densest fresh plumes were observed within the DWBC (σ_0 > 27.80) (**Fig. 10**). Using the data collected at 59.5°N, we showed that the fresh 'signals' originating from the shelf can be traced in the DWBC as far downstream as the latitude of Cape Farewell, where the anomalously fresh oxygenated plumes are repeatedly observed in the ISOW and DSOW density classes.

The results of our analysis along with the results from earlier studies [e.g., Rudels et al., 1999; Rudels et al., 2002] indicate that shelf water cascading in the northern Irminger Sea is an intermittent process occurring in all seasons of the year. This implies that, despite the apparent short duration of a particular cascading event, the cumulative contribution of such events to the thermohaline variability and southward export of the deep waters in the WBC can be considerable. Our tentative estimate based on data from two synoptic surveys at ~59.5°N suggests that the transient contribution of a cascading event in the northern Irminger Sea to the DWBC transport at Cape Farewell can be as large as ~25%.

References

1. Bacon, S. (1998), Decadal variability in the outflow from the Nordic seas to the deep Atlantic Ocean, *Nature*, *394*, 871–874.
2. Dickson, R. R., and J. Brown (1994), The production of North Atlantic Deep Water: Sources, rates and pathways, *J. Geophys. Res.*, *99*, C6, 12319–12341.
3. Dickson, R., Yashayaev, I., Meincke, J., Turrell, B., Dye, S., and J. Holfort (2002), Rapid freshening of the deep North Atlantic Ocean over the past four decades, *Nature*, *416*, 832–837.
4. Boessenkool, K. P., Hall, I. R., Elderfield, H., and I. Yashayaev (2007), North Atlantic climate and deep-ocean flow speed changes during the last 230 years, *Geophys. Res. Lett.*, *34*, L13614, doi:10.1029/2007GL030285.
5. Curry, R., Dickson, R., and I. Yashayaev (2003), A change in the freshwater balance of the Atlantic Ocean over the past four decades, *Nature*, *426*, 826–829.
6. Falina, A., A. Sarafanov, and A. Sokov (2007), Variability and renewal of Labrador Sea Water in the Irminger Basin in 1991–2004, *J. Geophys. Res.*, *112*, C01006, doi: 10.1029/2005JC003348.
7. Falina A., A. Sarafanov, H. Mercier, P. Lherminier, A. Sokov, and N. Daniault (2012), On the cascading of dense shelf waters in the Irminger Sea, *J. Phys. Oceanogr.*, doi:http://dx.doi.org/10.1175/JPO-D-12-012.1 (in press)
8. Hansen, B., Osterhus S., Quadfasel D., and W. Turrell (2004), Already the day after tomorrow?, *Science*, *305*, 953–954.
9. Hurrell, J. W. (1995), Decadal trends in the North Atlantic Oscillation: regional temperatures and precipitation, *Science*, *269*, 676–679.
10. Koltermann, K. P., A. Sokov, V. Tereschenkov, S. Dobroliubov, K. Lorbacher, and A. Sy (1999), Decadal changes in the thermohaline circulation of the North Atlantic, *Deep Sea Res.*, *Part II*, *46*, 109–138, doi:10.1016/S0967-0645(98)00115-5.
11. Lherminier, P., H. Mercier, T. Huck, C. Gourcuff, F. F. Perez, P. Morin, A. Sarafanov, and A. Falina (2010), The Atlantic Meridional Overturning Circulation and the subpolar gyre observed at the A25–Ovide section in June 2002 and 2004, *Deep-Sea Res.*, *Part I*, *57*, 1374–1391, doi:10.1016/ j.dsr.2010.07.009.

12. Meehl, G. A., (2007), Global climate projections. Climate Change 2007: The Physical Science Basis, S. Solomon et al., Eds., Cambridge University Press, 747–847.
13. Pickart, R. S., Spall, M., Ribergaard, M. H., Moore, G. W. K. and R. Milliff (2003), Deep convection in the Irminger Sea forced by the Greenland tip jet, *Nature*, *424*, 152–156.
14. Rudels B., Eriksson P., Grönvall H., Hietala R. and Launiainen J. (1999), Hydrographic Observations in Denmark Strait in Fall 1997, and their Implications for the Entrainment into the Overflow Plume, *Geophys. Res. Lett.*, *26*, 1325–1328.
15. Rudels, B., E. Fahrbach, J. Meincke, G. Budeus, and P. Eriksson (2002), The East Greeenland Current and its contribution to the Denmark Strait overflow, *ICES J. Marine Science*, *59*, 1133–1154.
16. Sarafanov, A., A. Sokov, A. Demidov, and A. Falina (2007), Warming and salinification of intermediate and deep waters in the Irminger Sea and Iceland Basin in 1997–2006, *Geophys. Res. Lett.*, *34*, L23609, doi:10.1029/2007GL031074.
17. Sarafanov, A., A. Falina, A. Sokov, and A. Demidov (2008), Intense warming and salinification of intermediate waters of southern origin in the eastern subpolar North Atlantic in the 1990s to mid-2000s, *J. Geophys. Res.*, *113*, C12022, doi:10.1029/2008JC004975.
18. Sarafanov, A. (2009), On the effect of the North Atlantic Oscillation on temperature and salinity of the subpolar North Atlantic intermediate and deep waters, *ICES J. Marine Science*, *66 (7),* 1448–1454, doi:10.1093/icesjms/fsp094.
19. Sarafanov, A., A. Falina, H. Mercier, P. Lherminier, and A. Sokov (2009), Recent changes in the Greenland–Scotland overflow-derived water transport inferred from hydrographic observations in the southern Irminger Sea, *Geophys. Res. Lett.*, *36*, L13606, doi:10.1029/2009GL038385.
20. Sarafanov A., A. Falina, P. Lherminier, H. Mercier, A. Sokov, and C. Gourcuff (2010a), Assessing decadal changes in the Deep Western Boundary Current absolute transport southeast of Cape Farewell (Greenland) from hydrography and altimetry, *J. Geophys. Res.*, *115*, C11003, doi:10.1029/2009JC005811.
21. Sarafanov A., H. Mercier, A. Falina, A. Sokov, and P. Lherminier (2010b), Cessation and partial reversal of deep water freshening in the northern North Atlantic: observation-

based estimates and attribution, *Tellus*, *62A*, 80–90, doi:10.1111/j.1600-0870.2009.00418.x.

22. Sarafanov A., A. Falina, H. Mercier, A. Sokov, P. Lherminier, C. Gourcuff, S. Gladyshev, F. Gaillard, and N. Daniault (2012) Mean full-depth summer circulation and transports at the northern periphery of the Atlantic Ocean in the 2000s, *J. Geophys. Res., 117,* C01014, doi:10.1029/2011JC007572.
23. Schmitz, W. J., Jr., and M. S. McCartney (1993), On the North Atlantic Circulation, *Rev. Geophys.*, *31*, 29–49.
24. Schott, F. A., and P. Brandt (2007), Circulation and deep water export of the subpolar North Atlantic during the 1990s, *in Ocean Circulation: Mechanisms and Impacts*, *Geophys. Monograph Series*, *173*, Eds. A. Schmittner, J. Chiang, and S. Hemmings, 91–118, doi:10.1029/173GM08.
25. Sutherland, D. A., and R. S. Pickart (2008), The East Greenland Coastal Current: structure, variability, and forcing, *Prog. Oceanogr.*, *78*, 58–77, doi:10.1016/j.pocean.2007.09.006.
26. Våge K., R. Pickart, A. Sarafanov, Ø. Knutsen, H. Mercier, P. Lherminier, H. van Aken, J. Meincke, D. Quadfasel, and S. Bacon (2011a), The Irminger Gyre: circulation, convection, and interannual variability, *Deep-Sea Res. Part I*, *58*, 590–614, doi:10.1016/j.dsr.2011.03.001.
27. van Aken, H. M. (2007), The oceanic thermohaline circulation: An introduction, New York, Springer, 326 p., ISBN 978-0-387-36637-1.
28. Yashayaev, I. (2007), Hydrographic changes in the Labrador Sea, 1960–2005, *Prog. Oceanogr.*, *73*, 242–276.

.

1.5 Preliminary Results

The upper-ocean, mid-depth and deep water circulation patterns, merging the results of the present analysis with those from the earlier studies [e.g., *Macrander et al.*, 2005; *Østerhus et al.*, 2005, 2008; *Schott and Brandt*, 2007; *Sutherland and Pickart*, 2008; *Lherminier et al.*, 2010; *Våge et al.*, 2011], are schematically visualized Figures 12–14. A schematic diagram of the meridional overturning circulation in the Atlantic Ocean north of 59.5°N is displayed in Fig. 9.

The results provide the following conceptual view of the gyre / overturning circulation at the northern periphery of the Atlantic Ocean in the 2000s.

The NAC and IC collectively carry 21.1 ± 1.0 Sv of warm upper-ocean waters across 59.5°N northwards within the MOCσ upper limb ($\sigma_0 < 27.55$). About 40% of this flow forms the Atlantic Inflow to the Nordic Seas, and 60% (12.7 ± 1.4 Sv) recirculates westwards in the subpolar gyre northern limb south of Iceland to feed the WBC in the Irminger Sea. Only 20% (2.4 ± 1.2 Sv) of the recirculating NAC/IC-derived waters exits the Irminger Sea in the WBC at shallow levels ($\sigma_0 < 27.55$), while 80% (10.2 ± 1.7 Sv, a half of the NAC/IC northward flow across 59.5°N) gains density of $\sigma_0 > 27.55$ and enters the MOCσ lower limb. The resulting net southward transport in the MOCσ lower limb at the latitude of Cape Farewell is 16.5 ± 2.2 Sv, of which ~60% (~10.2 Sv) is due to light-to-dense water transformation south of the GSR.

As no dense-to-light water re-conversion is expected to occur in the subpolar gyre, the NAC/IC-derived waters, once entering the MOCσ lower limb in the Irminger Sea, will eventually contribute to the MOCz lower limb (~11 Sv at 59.5°N) at the southern margin of the subpolar region. There, at ~48°N, the MOCσ and MOCz are of nearly the same magnitude, 16 ± 2 Sv, as estimated from data collected in the 1990s [see *Schott and Brandt*, 2007; *Lumpkin et al.*, 2008]. This is very close to our estimate of the mean MOCσ at 59.5°N. The comparison is tentative, though, because it does take into account the decadal variability of the MOC [*Koltermann et al.*, 1999; *Willis*, 2010]. With this caveat in mind, our results imply a minor contribution to the MOCσ by the net dense water formation in the subpolar gyre between ~48°N and 59.5°N. This inference concurs with the results by *Pickart and Spall* [2007] suggesting a

minor contribution to the Atlantic MOC by the net water mass transformation in the Labrador Sea.

To conclude, the results of the present study, verified with independent estimates where possible, provide the first observation-based quantitative view of a mean state of the gyre / overturning circulation at the northern periphery of the Atlantic Ocean. The most interesting features of the obtain circulation pattern are as follows:

• Nearly half of volume of the upper-ocean waters transported northward across 59.5°N in the eastern limb of the subpolar gyre (NAC and IC, $\sigma_0 < 27.55$) overturns in the density plane south of the GSR and feeds the lower limb of the Atlantic MOCσ.

• The contribution to the MOCσ lower limb at 59.5°N by overturning (light-to-dense transformation) of the NAC / IC-derived upper-ocean waters south of the GSR is one and a half times as large as the contribution of the Nordic Seas overflows.

• The net southward flow in MOCσ lower limb at 59.5°N is associated primarily with the deep water ($\sigma_0 > 27.80$) export. Nearly half of the net southward flow of deep waters across 59.5°N is due to entrainment of the Atlantic waters in the Irminger Sea.

• The DWBC at 59.5°N is fed primarily by the Denmark Strait Overflow and by the diapycnal flux / entrainment from the mid-depth layer, while the contribution to the DWBC transport from the ISOW flow is minor. A major part of the ISOW transported into the Irminger Sea from the Charlie-Gibbs Fracture Zone recirculates southward in the eastern Irminger Sea and exits the basin via an interior pathway rather than along the western boundary. The results can be used for validation of numerical models. From this perspective, multi-year mean transports have an obvious advantage over individual section-based synoptic estimates, which bear the impress of vigorous variability occurring on a variety of spatial and temporal scales. The methodological outcome is that the combined use of repeat hydrography, the MDT by *Rio and Hernandez* [2004] and satellite altimetry data can provide a useful estimate of the mean full-depth circulation across a transatlantic section without imposing *a priori* constraints.

1.6 Major Problems and Goals Not Achieved

Bottle ## 17 and 18 leaked at the first two stations. Seasave did not work properly on sta. 3383.

2. CONTINUOUS MEASUREMENTS (on station and underway)

2.1 Navigation

Navigation data from Trimble SPSx50/SPSx51 GPS was recorded every 1 second and was stored on the PC in binary format.

2.2 Meteorological Measurements

The standard mean meteorological measurements were stored in the separate files on the same PC with navigation data. Recording were running immediately after departure from Gdansk (Poland) on 12th June, and worked reliably until completion of the cruise in Halifax (Canada) on 5th July. Variability of the atmospheric pressure, air temperature relative humidity and winds during this time are shown in Figures 11-14.

2.3 Thermosalinograph

SBE 21 S/N 3254 data were collected along the section line starting on June 16th.

2.4 Echosounding

The bathymetric equipment aboard during RV Akademik Ioffe Cruise 49 consists of an ELAC 12 kHz hydrographic echosounder. Data were collected for most of the cruise. The Hull mounted transducer is located 5.8 metres below the sea surface and this value was entered to estimate the depth.

Depth was indicated on the echosounder display and stored on the PC together with the navigation.

Two files with extension NAV and MET with maximum size 256032 b were created. File name corresponded to GMT time when the file was opened for records.

2.5 Vessel Mounted Acoustic Doppler Current Profiler (VMADCP) OS 38 kHz

The Ocean Surveyor 38 kHz is designed for vessel-mount current profile measurement in the upper ocean water from depths greater than 40-50 meters. The system consists of a transducer and electronics chassis connected to PC. Data are transmitted in binary format through the I/O cable. GPS data in NMEA format are transmitted separately to another PC COM – port. The VMADCP can operate in two regimes (Narrow Bandwith and Broad Bandwith Profiling). Its main specifications are shown below.

To collect OS 38 kHz data we used *VmDas* software (version 1.46). The NMEA messages *VmDas* reads are standard GGA, HDG, HDT, VTG messages.

	Bin size	Maximum range	Accuracy $(cm/s)^2$
Narrow Band (long-range mode)	16 m	800 - 1000 m	30
	24 m	900 - 1200 m	23
Broad Band (high-precision mode)	16 m	520 - 730 m	12
	24 m	730 – 780 m	9

We used a following configuration to collect the data.

WP00001 – Broad Bandwidth profiling
WN045 – number of bins 45
WS2400– cell size 24 m
WF1600 – blanking size 16 m
BP00 – no bottom track (BP),

VmDas saves data in a few files with extension ENX, ENS, ENR (raw data with and without navigation), NR – NMEA messages, STA and LTA averaged data. Misalignment angle was introduced in configuration file and was used by VmDas for data correction.

Data processing performed STA files with 40-profile averaging. Taking into account that single ping takes about 3 seconds, one 40-profile ensemble lasts near 120 seconds in Narrow Bandwidth regime.

Data processing consists of data conversion in NetCDF format with extension NC and further cleaning, filtering, tide removing (using barotropic tidal model TPXO 7.2) and averaging. The standard averaging was 3 km. IFREMER software was used to process OS 38 kHz data.

3. ON-STATION MEASUREMENTS

3.1 CTD

3.1.1 Equipment

The deep profiler system used during the cruise included the following components: SBE 32 painted aluminum 24 bottle multisampler frame, SBE 9P-0743 CTD, Up and Down looking RD Instruments WHS – 300 kHz Acoustic Doppler Current Profiler (LADCP), Separate Battery pack pressure case ext. 6000 m connected to LADCPs with star cable, 24 x 5 liter Test Oceanic Niskin bottles, Benthos altimeter PSA-900D.

Lab equipment for data acquisition and archiving of CTD/LADCP data consisted of the following items mounted on the deck.

Pentium IV – Intel 2.2 GHz, PC Intel Core 2 Duo 2.4GHz Personal Computers. APC Back-UPS 550VA/330W, SBE 11p Deck Unit.

Cruise Preparation

Equipment and sensors were assembled when the ship crossed the Baltic and North Seas (12-16th June). Water bottles were checked for integrity of seals, taps, stoppers and lanyards before being fitted and roped to the multisampler frame.

Deployment

The CTD was deployed with a lowering rate of 60 meters/min (30-40 meters/min in the upper 200 meters or deeper if the conditions are rough). It is recovered at a rate of 60 meters/min.

The LADCPs fitted within the frame with a separate battery pressure case performed well. These units contain a compass and tilt sensors which could possibly provide useful information on the attitude and rotation of the whole profiler package throughout deployments.

Bottle firing using the deck unit and pylon was very reliable during the cruise.

Operationally this has been a successful cruise with virtually no time being lost due to mechanical or equipment failure.

3.1.2 Data processing and calibration

CTD data were logged at 24 scans per second and passed from the CTD deck unit to the PC.

The CTD data was recorded onto disk by the PC using SEABIRD SEASOFT-Win 32: Seasave 7, Software Release 7.21d. A screen display of temperature, oxygen, salinity and density profiles vs pressure are used to decide the depths at which bottles are to be tripped on the up cast. The bottles are tripped using the enable and fire buttons on the PC screen. During post-processing, the SEASAVE software stores 35 scans at each bottle trip within a separate file. At the end of the station, all the data and header files associated with the station are transferred immediately via ethernet to the second PC. The SBE data processing software is used to create 1 dbar processed data files.

The data processing takes the following steps:

DATCNV Converts the raw data to physical parameters.

WILDEDIT For every block of 100 scans, flags all scans whose pressure, temperature, conductivity and oxygen values differ from the mean by more than 2 standard deviations. Recomputes mean from unflagged data then marks as bad all scans exceeding 20 standard deviations from these new values.

FILTER Low pass filter pressure channel with time constant used for pressure 0.150 seconds.

ALIGNCTD Aligns the oxygen values relative to the pressure values accounting for the time delays in the system. Time offsets of 4.000 secs for oxygen are used.

CELLTM A recursive filter used to remove the thermal mass effects from the conductivity data. Thermal anomaly amplitude and time constants of 0.0300 and 7.0000 were used.

LOOPEDIT Marks as bad, all cycles on the down trace for which the vertical velocity of the CTD unit is less than 0.25 metres/sec.

WINDOW FILTER cosine filter temperature and conductivity, window size 23 scans.

DERIVE Computes salinity, potential temperature, sigma-t, sigma theta and oxygen values.

BINAVG Averages the down cast into 1 dbar pressure bins.

SPLIT Splits the data into DOWN and UP cast.

Calibration data

The CTD calibrations used during this cruise were supplied by Sea Bird Electronics and are as follows:

Pre-cruise calibration:

CALIBRATION DATE: 04-Jun 2015 (all stations)

Conductivity Sensor S/N 042827

g = -1.00469063e+001
h = 1.37383902e+000
i = -6.26359501e-004
j = 1.11707771e-004

CPcor = -9.5700e-008
CTcor = 3.2500e-006

Post-cruise calibration:
CALIBRATION DATE: 19-May 2016 (all stations)
Conductivity Sensor S/N 042827
g = -1.00334013e+001
h = 1.36943454e+000
i = 5.51582754e-004
j = 2.66453767e -005

CPcor = -9.5700e-008
CTcor = 3.2500e-006
Average drift between *pre* and *post-cruise* calibrations: +0.00015 PSU/month

Pre-cruise calibration:
CALIBRATION DATE: 19-Jun-14 (all stations)
Temperature Sensor S/N 035677
Temperature ITS-90 = 1/{g + h[*ln*(f0/f)] + i[*ln*2(f0/f)] + j[*ln*3(f0/f)]} - 273.15 (°C)
Following the recommendation of JPOTS: T68 is assumed to be 1.00024 * T90 (-2 to 35°C)
f is the frequency
g =4.29395484e-003
h =6.23609246e-004
i =1.89843091e-005
j =1.41258435e-006
f0 = 1000.0

Post-cruise calibration:
CALIBRATION DATE: 20-Jun-16 (all stations)
Temperature Sensor 035677
g = 4.29377606e-003
h = 6.23241122e-004
i = 1.87210995e-005
j = 1.34957544e-006
f0 = 1000.0
Average drift between *pre* and *post-cruise* calibrations: -0.00029 Degrees Celsius/year

Pressure Sensor S/N 89105 (all stations) no drift
CALIBRATION DATE: 27-June-11
C1 = -4.9053 7 1 e+004
C2 = -1.2105 9 4 e+000
C3 = 1.4283 5 0 e-002
D1 = 3.9016 0 0 e-002
D2 = 0.0000 0 0 e+000
T1 = 3.0010 1 7 e+001
T2 = -5.7583 8 4 e-004
T3 = 4.2101 2 0 e-006
T4 = 2.2654 0 0 e-009
T5 = 0.0000 0 0 e+000)
AD590M = 1.28912e-002

AD590B = -8.43097e+000
Slope = 0.99995
Offset = 1.4284 (dbars)

Oxygen Sensor 430699
CALIBRATION DATE: 23-Jul-2015 (All Stations)

The final coefficients are for deep ocean (sta 3330 – 3391)

Soc = 4.4260e-001
Tau = 0.0
Boc = 0.0000
Voffset = -0.4598
tcor = 0.001700
pcor = 1.35e-004

For Greenland shelf and East Greenland Current (sta 3391 – 3414)

Soc = 4.3627e-001
Tau = 0.0
Boc = 0.0000
Voffset = -0.4048
tcor = 0.001700
pcor = 1.35e-004

3.1.3 Final Post-Cruise CTD Calibrations

Temperature Calibration Temperature Sensor 035677

-0.00029 sensor drift was applied to the temperature data based on the *pre cruise calibration coefficients* for all stations.

Pressure Calibration Pressure Sensor S/N 89105

Final CTD pressure correction: Since no drift for pressure sensor was defined by SeaBird Electronics pressure was corrected for atmospheric pressure only. With offset in *.con* or *.xmlcon* file set to -0.0026 db, pressure measured by CTD should equal barometric pressure

• Calculate offset (db) = barometer reading – CTD reading

– Conversion of psia to decibars: decibars = (psia - 14.7) * 0.6894759

• Enter calculated offset in *.con* or *.xmlcon* file

• Example:

– CTD reads -2.5 dbars

– Barometer reads 14.65 psia.

Converting to decibars, barometer reads (14.65 - 14.7) * 0.6894759 = -0.034 dbars

– offset (db) = barometer reading – CTD reading = -0.034 - (-2.5) = 2.466

Salinity Calibration Conductivity Sensor 042827

We used *pre-cruise calibration coefficients* with slope correction 0.9999977 for all stations of the cruise, which is equivalent salinity correction by -0.0001 PSU.

3.1.4 SBE 43 Dissolved Oxygen Sensor Calibration using Winkler Titrations

We use a method for statistically estimating calibration coefficients for calculating dissolved oxygen in milliliters per liter from SBE 43 output voltage. The technique requires dissolved oxygen concentration in ml/l (determined from Winkler titration of water samples) and SBE 43 oxygen voltage outputs at the times the water samples were collected. Sea-Bird's data processing software, SBE Data Processing, is used to produce a data table suitable for the analysis.

Background

The equation used in Sea-Bird's software for calculating dissolved oxygen in ml/l from SBE 43 output voltage is a form of that given in Owens-Millard (1985):

$$Oxygen\ (ml/l) = \left\{ Soc * \left(V + Voffset + tau(T,P) * \frac{\partial V}{\partial t} \right) \right\} * Oxsol(T,S) * \left(1.0 + A*T + B*T^2 + C*T^3\right) * e^{\left(\frac{E*P}{K}\right)} \qquad eqn\ 1$$

where:

- V = SBE 43 output voltage signal (volts)
- $\partial V/\partial t$ = time derivative of SBE 43 output signal (volts/second), computed over a default window of 2 seconds
- T = CTD temperature (°C)
- S = CTD salinity (psu)
- P = CTD pressure (dbars)
- K = CTD temperature (°K = °C + 273.15)
- *tau(T,P)* = sensor time constant at temperature and pressure
- *Oxsol(T,S)* = oxygen solubility function (ml/L), which converts oxygen partial pressure (sensor measurement) to oxygen concentration (*Garcia and Gordon, 1992*). See Appendix A in *Application Note 64: Background Information, Deployment Recommendations, and Cleaning and Storage* for values at various temperatures and salinities.
- *Soc, Voffset, A, B, C, E*, and *tau20, D1, D2* [terms in calculation of *tau (T,P)*] are calibration coefficients

The SBE 43 is expected to provide an output voltage that is linear with respect to oxygen concentration. Normal calibration drift manifests itself as a loss of sensitivity and is evident as a change of slope (and less so in offset) in the linear relationship between oxygen concentration and voltage output. The coefficients *A, B, C,* and *E* correct for small secondary responses to temperature and pressure. Because these coefficients change very slowly over time, the values given on the SBE 43 calibration certificate will be used in this analysis, and we will concern ourselves with estimating changes in the slope (Soc) and offset (Voffset).

Setting $\frac{\partial V}{\partial t}$ to zero, we rearrange equation 1 into a linear form and perform a linear regression to obtain a new *Soc* and *Voffset*.

Let:

$$\phi = Oxsol(T,S) * \left(1.0 + A*T + B*T^2 + C*T^3\right) * e^{\left(\frac{E*P}{K}\right)} \qquad eqn\ 2$$

The oxygen equation then reduces to the form in equation 3:

$$Oxygen(ml/l) = Soc * (V + Voffset) * \phi \qquad eqn\ 3$$

This may be expressed in a linear form in equation 4.

$$\frac{Oxygen(ml/l)}{\phi} = Soc * (V + Voffset) = M * V + B \qquad eqn\ 4$$

Where:
Soc = M
Voffset = B / M

A linear regression is calculated using Winkler oxygen concentration divided by ϕ as the dependent variable and SBE 43 output voltage as the independent variable.

Winkler oxygen divided by φ versus SBE 43 output voltage for this cruise is shown in

Fig. 14 and includes a linear regression line calculated from the data.

The *Soc* = 4.4260e-001
The *Voffset* = -0.4598 for the transatlantic section along 59.5 N
1202 oxygen samples were used to build this linear fit for the 59.5 N line.

The *Soc* = 4.3627e-001
The *Voffset* = -0.4048 for the Greenland shelf
263 oxygen samples were used to build this linear fit.

Procedure

The linear regression that yields a new *Soc* and *Voffset* may be accomplished with spreadsheet software, a hand-held calculator with statistical capability, or (with perseverance) a calculator, graph paper, and pencil. As a first step, extract pressure, temperature, salinity, oxygen saturation, and SBE 43 voltage from the parts of your CTD data collected when the water sampler closures occurred.

Run SBE Data Processing, and select Data Conversion in the Run menu. Select the appropriate configuration (*.con*) and data (*.dat* or *.hex*) files on the *File Setup* tab. Click the *Data Setup* tab and set *Convert data from* to *Upcast and downcast* and *Create file types* to *Create bottle (.ros) file only*.

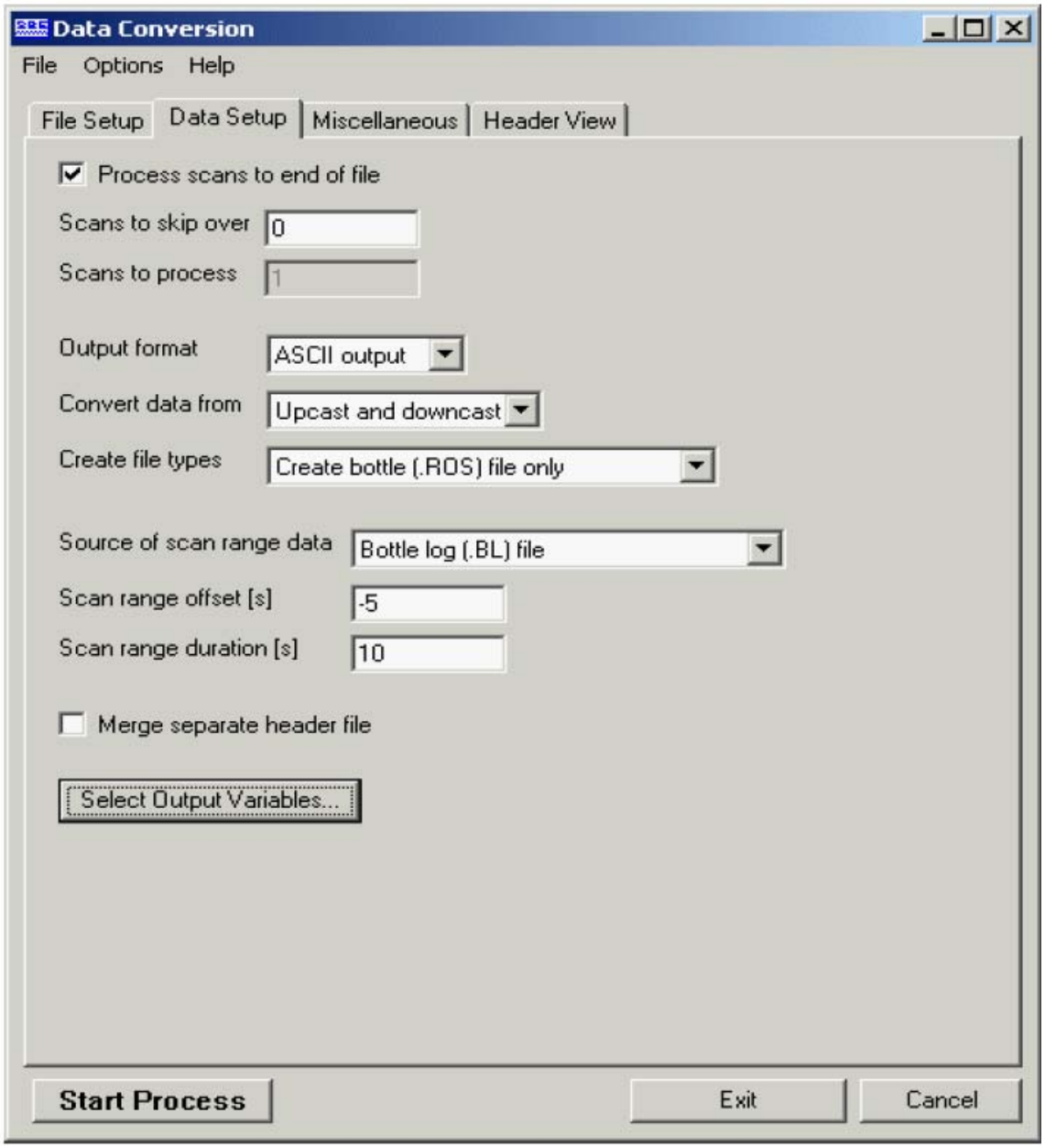

To extract CTD data concurrent to the water sampler closures, Data Conversion must know when the closures occurred. Select an appropriate *Source of scan range data*, depending on your instrument type and how the sampler was commanded to close bottles:

- SBE 9*plus* with SBE 11*plus* or 17*plus* - The data stream is marked with a *bottle confirm* bit each time a closure occurred.
- Using SEASAVE to operate the water sampler - A *.bl* file, with scan ranges corresponding to closures, is created during the cast.
- SBE 19, 19*plus*, 19*plus* V2, or 25 with Auto Fire Module (AFM) and SBE 32 Carousel Water Sampler, or operated autonomously with SBE 55 ECO Water Sampler - The *.afm* file contains scan ranges.

Like all sensors, the SBE 43 has a finite response time to a change in dissolved oxygen concentration. This response time is usually on the order of 6 seconds. For this reason, good sampling procedure dictates that the instrument package should be stopped in the water column long enough for the SBE 43 and all other sensors to completely equilibrate before closing the water sampler. An equilibration time of 5 to 6 response times, or 30 to 36 seconds, is adequate.

In the example above, Data Conversion will begin extracting data 5 seconds before each water sampler closure (*Scan range offset = -5 s*) and will extract a total of 10 seconds of data (*Scan range duration = 10 s*). Note that 10 seconds is longer than the SBE 43 response time. Because we are extracting data for 5 seconds after the water sampler closure, the instrument package must remain stopped for at least this long.

To estimate *Soc* and *Voffset*, you need pressure, temperature, salinity, oxygen saturation (ml/l), and SBE 43 Oxygen Voltage to go with each Winkler titration data value. Click *Select Output Variables* and add each of the required parameters; the dialog box is shown below.

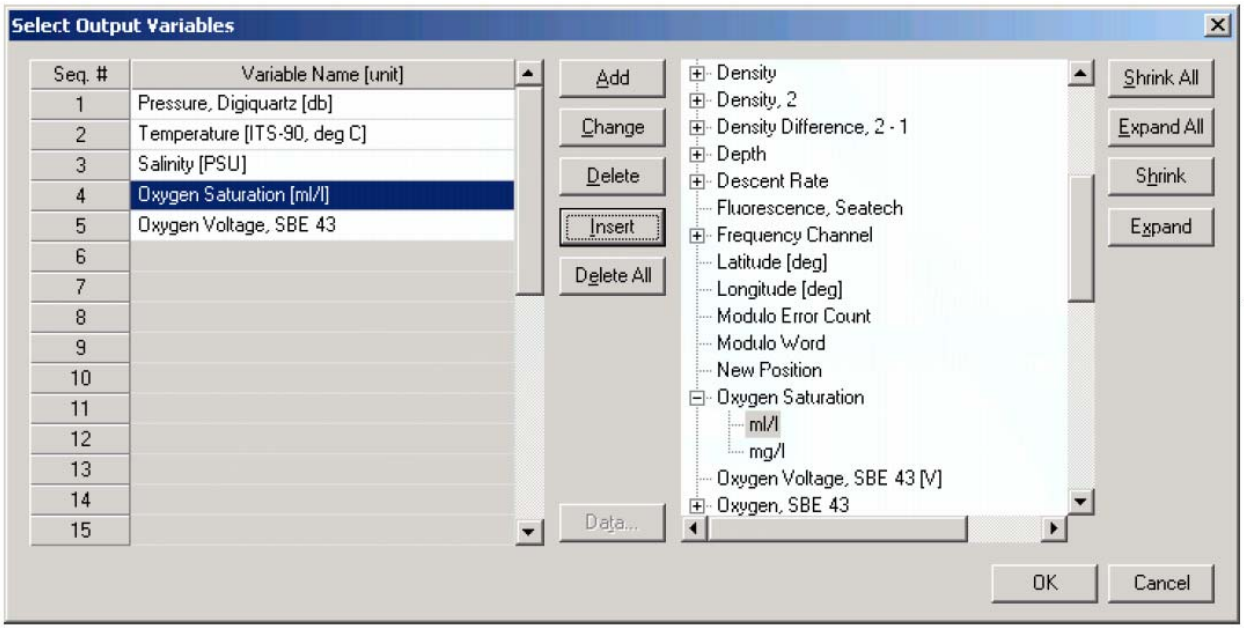

After selecting all the variables, click *OK* to return to the Data Conversion Data Setup tab. Then click *Start Process* to create the *.ros* file.

For this example, the *.ros* file contains 10 seconds of data centered on the moment the bottle closure occurred for every bottle closure. To make a useful table, select Rosette Summary from SBE Data Processing's Run menu. Rosette Summary calculates averages and standard deviations for the variables selected in Data Conversion. Select the appropriate *.con* and *.ros* files on the *File Setup* tab. Click the *Data Setup* tab and then click the *Select Averaged Variables* button; the dialog box is shown below.

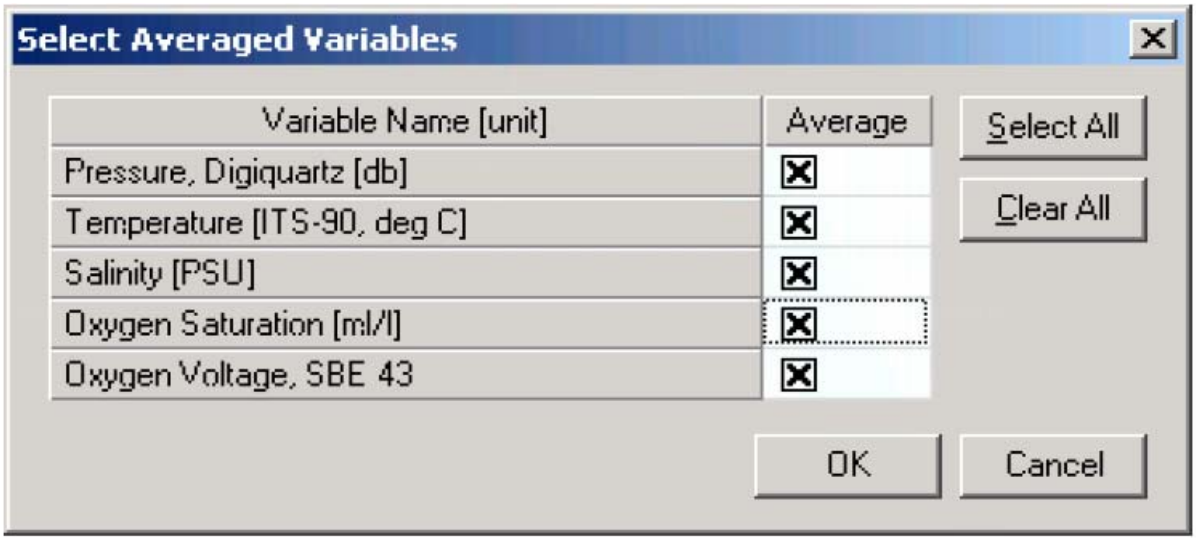

After selecting all the variables, click *OK* to return to the Rosette Summary Data Setup tab. Then click *Start Process* to create a data table file with the *.btl* extension.

Create a table with average pressure, temperature, salinity, oxygen saturation, and SBE 43 output voltage for each water sampler closure depth, by importing the *.btl* file into a spreadsheet. Then, enter by hand the Winkler titration dissolved oxygen values from your titration log, matching water sampler closures to pressures.

Calculate $\phi = Oxsol(T,S) * \left(1.0 + A*T + B*T^2 + C*T^3\right) * e^{\left(\frac{E*P}{K}\right)}$,

using *A, B, C,* and *E* from the SBE 43 calibration sheet.
Then, calculate $Winkler\ O_2 / \phi$.

Perform a linear regression, with:

- $Winkler\ O_2 / \phi$ (shown as Winkler/phi in the table) as the *Y* data
- SBE 43 output voltages as the *X* data

If a spreadsheet or statistical calculator is not available, the regression equations are:

$$M = \frac{n * \sum\left(V * \frac{Winkler\,O_2}{\phi}\right) - \sum V * \sum\left(\frac{Winkler\,O_2}{\phi}\right)}{n * \sum V^2 - \left(\sum V\right)^2}$$

$$B = \frac{\sum\left(\frac{Winkler\,O_2}{\phi}\right) - M * \sum V}{n}$$

Where:
n = number of data pairs
M = Slope
B = Offset

And:
$Soc = M$
$Voffset = B/M$

Reference

Owens, W. B., and R. C. Millard Jr., 1985: A new algorithm for CTD oxygen calibration. J. Phys. Oceanogr., 15, 621-631.

(NOTE: calibration expressed as ml/l)

3.2 Oxygen Bottle Samples

Oxygen samples were drawn first from every bottle. Duplicate samples were taken on each cast, usually from the first two bottles. Samples were drawn into clear, wide necked calibrated glass bottles and fixed on deck with reagents dispensed using Aquastep bottle top dispensers. A test station used to check on the oxygen bottle calibrations and as an opportunity to train a number of people to take the samples. The samples were shaken on deck and again in the laboratory 1/2 hour after collection, when

the bottles were checked for the tightness of the stoppers and presence of bubbles. The samples were then stored under water until analysis.

Bottle temperatures were taken, following sampling for oxygen, using a hand held electronic thermometer probe. The temperatures were used to calculate any temperature-dependent changes in the sample bottle volumes.

Samples were analyzed in the constant temperature laboratory, starting three hours after sample collection, following the Winkler whole bottle titration with an amperometric method of endpoint detection, as described by Culberson (1991). The equipment used was supplied by Metrohm and included the Titrino unit and control pad, exchange unit with 10 ml burette to dispense the thiosulphate in increments of 2 μl , with an electrode for amperometric end point detection.

The difference for the duplicate pairs sampled on each station was in a range 0.00-0.02 ml/l .

The thiosulphate normality was checked on each run and recalculated every time the reservoir was topped up against potassium iodate. The exact weight of this standard, the calibrated 5 ml exchange unit driven by a Metrohm Dosimat and the 1L glass volumetric flask used to dispense and prepare the standard.

The introduction of oxygen with the reagents and impurities in the manganese chloride were corrected for by blank measurements made on each run, as described in the WOCE Manual of Operations and Methods (Culberson, 1991).

Collected data shows that dissolved oxygen concentrations varied from 4.25 to 9.47 ml/l. In order to control the accuracy of the oxygen measurements at each cast were taken parallel samples from the 1-2 bottles or duplicate samples.

Reproducibility of measurements

1465 samples were taken during the cruise; in addition 53 duplicates were analyzed. These include both duplicates taken from the same bottle (replicates) and those taken from different bottles fired at the same depth. The data gave a standard deviation of 0.007 ml/l.

3.3 Nutrient Bottle Samples

Samples for nutrient measurements were collected following oxygen samples from each Niskin bottle. Water was collected in clean plastic containers that had been rinsed three times by seawater through the latex tube.

Concentrations of silicate and phosphate were determined by photometric methods with spectrophotometer Cary 100 Seam Varian. All samples were analyzed immediately after sampling.

Silicate determined by Korolev's method based on colorimeter of blue silicomolybdic complex (methodology described in Modern methods..., 1992). The ascorbic acid used as a restorative. The absorbance was read at 810 nm. Relative error of this method on concentration of dissolved silicate at 4.5 μM is ±4%, on concentration at 45 μM - ± 2,5%. Measured concentrations were in a range from 0.20 to 20.71 μM.

Phosphates determined according to the method Murphy and Raily (Modern methods..., 1992). Phosphate, dissolved in sea water, react with ammonium molibdate in a presence of sulfuric acid and tartrate potassium-antimony. The generated complex aggregate of phosphomolybdic heteropolyacid and trivalent antimony restorative by the ascorbic acid, and then determined the absorbance at 885 nm (we use the cavity 10cm). Relative error of this method ± 1%.

In order to ensure accuracy and increase precision of determination 3-8 duplicate samples were analyzed at each run. The mean difference for the duplicate pairs sampled on each station was in an error limits of the methods.

References:

Culberson, C.H. 1991.15 pp in the WOCE Operations Manual (WHP Operations and Methods) WHPO 91/1, Woods Hole.

Modern methods of hydrochemical research of the ocean, 1992. IO RAS, Moscow (in Russian).

3.4 Lowered Acoustic Doppler Current Profiler (LADCP)

The TRDI WHS 300 kHz ADCPs consists of a pressure case rated to 6000 meters with 4 transducers at one end in a convex arrangement and the beams diverging at 20 degrees from the vertical. At the opposite end to the transducers is a connector that enables downloading of data and connects it to other pressure cases containing another ADCP and the power supply pack. This arrangement allowed the ADCPs and the battery pack to be mounted vertically as up and down-looking on the CTD frame. Connection amongst all units was established using star cable with three male and two female terminations. Two male cable ends were always attached to the frame, this enabled comms leads to be readily connected pre and post deployment.

Communications: The 20-m communication leads (which also allow external power to be supplied to the ADCP) were sufficiently long to route it through to the port side of the deck lab where it was connected to a dedicated PC and external power supply. The latter was set at 48+ volts and was left on

whilst the ADCP was on deck. 5 minutes prior to deployment the external power supply was shut off, the instrument checked and the configuration file sent to the ADCP as described in the manual instructions. The free end of the fly leads was greased and the end cap refitted, this was then taped to the frame for security.

Post deployment: When the CTD/LADCP was brought inboard, the fly-lead connectors were dried and the comms leads were connected to them. This stopped undue bending of the cables and kept them clear of the water bottles, aiding sampling. External power was applied again and the cast data downloaded as per the manual with a baud rate of 57600. The processing is accomplished using software developed by Visbeck after transferring the data to the PC.

Battery power was supplied to the ADCP in the form of 42 volts from 28 x 1.5 volt alkaline cells. Four of these packs were available for the cruise, as the ADCP will function at a minimum of 32 volts this was deemed an adequate stock for the duration.

Data quality: The data quality from the ADCP was good throughout. Due to the bad weather instrument titles sometimes exceeded 12° and this data was rejected during processing.

The LADCPs seem to function well and generates useful information on currents. The battery supply has its limitations though and thought should be given to alternatives to the present set-up.

3.4.1 LADCP Processing for Current Profiles

A brief account of the LADCP current data processing, file nomenclature and directory structure is provided in the following lines. Little emphasis is put into a detailed description of the main programming tools used, since these are part of a standard software package developed by Gerd Krahmann (version 10.13).

Outline of LADCP current calculation method

The Broad Band LADCP used during AI49 cruise was designed to measure the instantaneous relative velocities of scatterers in the water column by taking advantage of the Doppler frequency shift, phase changes and correlation between coded pulses transmitted and received by the LADCP's four transducers. Conversion of this raw data stream to a profile of absolute currents involved an elaborate calculation method.

Firstly, Doppler shifts needed to be scaled to velocity units by taking into account the depth-dependent sound velocity (estimated from CTD T and S measurements). Directions could be inferred from trigonometric calculations based on the geometry of the transducer set, the orientation of the package (measured with a flux gate compass) and the local magnetic declination. The depth of the instrument was calculated from the integration of the measured vertical velocity and later adjusted to match the depth given by the CTD's pressure sensor.

The velocities corresponding to each single ensemble (or, in effect, to each transducer ping) were gridded in bins of depth set 10 meters. Statistical rejection of spiky measurements within each of these bins followed.

In order to reject the unwanted motion of the instrument (but also the barotropic component of the current), shear profiles were calculated for each ensemble. A complicated editing scheme preceded this shear calculation. A final shear profile (baroclinic current) was derived by real- depth gridding of the shear profiles calculated for individual ensembles. It was hoped that any relative velocities introduced by the high-frequency motion of the CTD package would be smoothed out by this repeated averaging.

The barotropic component of the flow was finally calculated from bottom-tracking measurements (bottom-track mode) or, in most occasions, in an integral sense from differential GPS positions of the ship (water-track mode).

The definitive velocity profile was hence obtained as the sum of the baroclinic and barotropic components.

During AI49 cruise, no specific error calculation was performed. Profiles of shear standard deviation were included in the cast log sheet folder. Internal wave signals were obvious throughout the cruise.

Relevant PC files

The raw data were downloaded from the LADCP into a devoted PC after each cast and stored as a binary file called vNNNNm_01.000 for Master and vNNNNs_01.000 for Slave the c:\ladcp\AI49\dNNN directory, where NNNN stands for the CTD cast number, e.g. raw data from cast 3330 were stored in the files d:\AI49\data\ladcp\v3330m_01.000 and v3330s_01..000.

The configuration files (named Mconf.txt and Sconf.txt) containing the operating instructions (setting of track mode, bin depth, etc.) given to the LADCP previously to deployment was stored in the same directory.

Text files of the form NNNNm.log and NNNNs.log are the log of the 'bbtalk' session (testing the state and functioning of the instrument) previous to deployment. The details of the sessions for every single cast in the cruise are to be found in the cast log sheets.

A whole variety of files were created and manipulated during the different processing stages, and no mention will be made of the majority of them for reasons of clarity. The processing procedure may be summarised in two steps:

1- create CTD pressure, temperature and salinity data file as well as navigation collected every second in order to obtain the best possible estimates of depth and sound velocity. This is done using 'SBE Data Processing software and ConvLADCP Fortran program.

2- use the Gerd Krahmann's standard matlab package (v.10.13) with P. Lherminier's improvements (LPO, IFREMER) to process LADCP and CTD data

References

M. Visbeck 2002 Deep Velocity Profiling using Lowered Acoustic Doppler Current Profiler: Bottom Track and Inverse Solutions J. Atmos. Oceanic Technol. 10, 764-773.

3.5 Phytoplankton production in the North Atlantic

Subpolar North Atlantic is the region of high biological productivity, seasonal and interannual variability. North Atlantic ecosystem is very sensitive to the climate changes. Thus, improving of our representations about spatial and temporal variability of phytoplankton production characteristics is the necessary for understanding of carbon circle patterns and for primary production algorithms evaluations.

The main aims of the studies were:

1. Estimation of primary production and chlorophyll spatial variability and finding relations between phytoplankton production characteristics and circulation as well as patterns of hydrophysical and hydrochemical vertical structure.
2. Measurements of integral phytoplankton production characteristics at 59.5° N.
3. Study of vertical primary production and chlorophyll distribution.
4. Spatiotemporal primary production, chlorophyll and environmental factors database development.
5. Development of regional primary production models.
6. Improving the estimation of phytoplankton physiological condition by fluorescence methods.
7. Estimation of the dissolved organic matter contribution in primary production.
8. Research of light stress influence on phytoplankton photosynthetic activity.

Phytoplankton production parameters were collected on 80 CTD stations. Vertical distribution of chlorophyll was studied on 28 stations. Primary production was measured on 13 stations. 74 phytoplankton and 105 primary production samples were treated. Totally 328 measurements of pigment concentration were made respectively.

(Dr. A. Demidov)

3.6 Geological studies in the North Atlantic

The goal of this study was to describe the modern sediment system of the North Atlantic and to collect cores for a high-resolution reconstruction of climate change.

The research team had several objectives: an atmospheric aerosol study; collection of water samples to estimate the concentration and composition of suspended matter, including total and organic carbon, and phytoplankton pigments; collection of bottom sediment samples; microbiological and biogeochemical studies; and deployment of mooring stations (MS) (Figure 13, table 2).

Atmospheric aerosols. A TSI AeroTrak APC-9303-01 airborne particle counter, (United States) was used to obtain the granulometric spectrum of aerosol particles in the surface layer. The atmospheric suspended particulate matter in surface layer was sampled using nylon nets.

Suspended sediment matter. The water was sampled for suspended sediment studies at the surface along the ship's route and in the ocean interior at oceanographic stations. To estimate the total concentration of the suspended matter, seawater was filtered under a vacuum of –0.4 atm through preliminary weighted nuclear filters 47 mm in diameter (pore diameter of 0.45 μm). To find the concentration of suspended organic carbon and chlorophyll, filtration was done through preliminarily calcinated Whatman GF/F glass fiber filters with a diameter of 47 mm (effective pore size of approximately 0.7 μm) under a vacuum of –0.2 atm in order to remove organic substances. The filters for the total content of the suspended particulate matter were dried in situ, and the glass fiber filters for the calculation of chlorophyll content were frozen and transported in a container with silicagel to Moscow. The content of suspended organic carbon was calculated on an AN-7529 device at the Institute of Oceanology, Russian Academy of Sciences. The concentrations of phytoplankton pigments (chlorophyll a and pheophytin a) were determined by the fluorometric method using a Turner Trilogy fluorimeter, which was preliminarily gauged at the Chair of Biophysics of the Department of Biology, Moscow State University. The contents of Si, Al, and P were estimated by the photometric method.

Bottom sediments. Large samples of bottom sediments were extracted with an Okean-0.25 Grab Sampler (GS), and sediment cores were recovered with a Gravity Corer (GC). Three cores from the GC and 6 minicores from the GS were examined in total.

Microbiological studies. At key stations of the studied transect, a set of measurements was carried out to assess the activity of microbial carbon and serum transformation, including the intensity of microbial carbon dioxide assimilation and methanogenesis and sulfidogenesis efficiency. Some samples were collected to define the isotopic composition of organic and

mineral carbon in the suspended matter and bottom sediment. An express analysis was performed to assess the oxidation–reduction potential of sediment and the alkaline reserve of pore water.

Vertical fluxes of suspended matter were studied with sediment traps set in the MS. Three MS were mounted, where 5 large sediment traps Lotos-3 with 12 sample bottles and 30 integrated small sediment traps MSL-110 were installed. Teledyne RDI DVS-750 and DVS-6000 current meters were used to assess the horizontal flow component (Figures 14–16).

Preliminary results

Prevailing wind directions were northwest, north, and northeast during the entire transit along the transect. The granulometric spectrum of surface layer aerosols varies depending on the wind state. The most significant correlation between the number of particles and wind speed was found for the >1.0 fraction (0.6 when n = 22). The concentration and flux of sampled aerosol particles were 0.007 μg/m^3 and 11.9 μg/m^2, respectively. The inverse trajectories of air masses (HYSPLIT model) indicate that matter arrives from central Arctic reference areas.

Suspended matter concentrations were found to be in a range from 0.07 to 1.1 mg/L. The highest concentrations were observed rather close to the coast (North Sea and Greenland), but also in areas affected by the Irminger and North Atlantic currents. As for the vertical profiles, the highest concentrations were marked out in the upper ocean mixed layer (to a depth of 100 m), and for most of cases, at the surface (0 m). At some stations (3348, 3352), the suspended matter maximum was recorded in the subsurface layer (20–35 m). At nearly all stations, an increase in suspended matter concentration was found in the near-bottom layer.

The upper sediment layer consisted mainly of zooplankton carbon remains, which form light brownish coccolite foraminipheric clay. The pattern of active bioturbation was noted at every station. A large contribution to the composition of surface sediments came from ice rafting. Sediment core 3359 was 486 cm long, recovered by GC at a depth of 2517 m at the eastern end of the Gardar Drift, where sediment waves were observed. It consisted of high carbonate clay rich in foraminifera in the upper portion of the core (0–15 cm). The bottom part of the core is loamy silt with light brownish and grayish banding. The GC core 3378 was 466 cm long, recovered at 2192 m depth on the eastern slope of Reykjanes Ridge near the Snorri Drift, which is an area controlled by the bottom Iceland–Scotland Overflow along the ridge to its south. The core consists of rather homogeneous light brownish silt rich in carbonate material, and the ice rafting pattern is continuous. The GC core 3415 was 507 cm long, recovered at 2985 m in the western part of the Gloria Drift on the boundary between the Irminger and Labrador basins. Light brownish silt with a high concentration of carbonate material was discovered.

The oxidation–reduction potential was positive all along the collected sediment core. At the same time, the Eh value decreased by 25–45 mV from the upper to the deeper part of the core, which suggests that microbial oxidation of organic matter was taking place with oxygen consumption. Apparently, the activity of microbial processes attenuates deeper into the sediment. A weak increase in the alkaline reserve of pore water is noted deeper into the sediment.

(Dr. N. Politova)

. CRUISE LOGISTICS

Mobilization

Mobilization for the cruise took place on the way from Gdansk (Poland) to the first station of the cruise. It took four days. The scientific team arrived at the ship on June 11th.

ACKNOWLEDGEMENTS

The principal scientists would like to thank the Master, officers, crew and scientists of the RV Akademik Ioffe for making this such an enjoyable, as well as successful cruise.

TABLES

FIGURES

Fig. l Station location and ship track (in red). The shelf area with depth less than 200 m is shaded

Fig.2 Vertical distribution of samples along the 59.5 section.

Fig. 3. Schematic diagram of the large-scale circulation in the northern North Atlantic compiled from [Schmitz and McCartney, 1993; Schott and Brandt, 2007; Sutherland and Pickart, 2008; Lherminier et al., 2010]. Abbreviations for the main topographic features, currents and water masses are explained in the legend. The nominal locations of the 59.5°N hydrographic section (1997 – present) and sections across the straits between Greenland, Iceland, Faeroe and Shetland Islands (2011 – present) are shown with the solid green lines.

Fig. 4. Oxygen concentrations (ml/l) in the water column (lower panel) as observed in March–October 1997 in four hydrographic sections (upper panel) ending nearby the southern tip of Greenland. A separate oxygen maximum in the LSW layer (1000–2000 m) in the Irminger Sea at 59.5°N strongly implies local convective renewal of LSW before 1997. Adapted from [Falina et al., 2007].

Fig. 5. Warming and salinification in the northern North Atlantic between the mid-1990s and mid-2000s, as observed at 59.5°N. The figure shows the 2006–1997 temperature (°C, left) and salinity (right) differences on isobaric surfaces in the Irminger Sea and Iceland Basin. Adapted from [Sarafanov et al., 2007].

Fig. 6. Coherence of the decadal salinity changes (1950s – 2000s) of the intermediate (LSW) and deep (ISOW) waters in the northern North Atlantic and their link to the North Atlantic Oscillation (NAO) index. **(a)** Schematic representation of the LSW and ISOW pathways and locations of the Icelandic Low (L) and Azores High (H) centers constituting the NAO dipole pattern. The red dotted line indicates the 59.5°N transatlantic section. **(b)** Salinity time series for LSW in the Labrador Sea [Yashayaev, 2007] and ISOW in the Iceland basin [Boessenkool et al., 2007; Sarafanov et al., 2007] overlaid by the third order polynomial fits. **(c)** Time series of the winter NAO index, after [Hurrell, 1995], overlaid by 7-year running mean and third order polynomial fit. **(d)** Mechanism of the NAO effect on the decadal changes in temperature (T) and salinity (S) of the northern North Atlantic intermediate and deep waters. Positive / negative links shown with the dark / light grey arrows mean that changes in 'causative' and 'consequential' characteristics have the same / opposite sign(s). The overall effect of the NAO on T and S of the in the water column is negative: persistent NAO decline leads to warming and salinification of the water masses and vice versa, as shown in (b) and (c). Adapted from [Sarafanov, 2009].

Fig. 7. Schematic representation of the upper-ocean circulation and convection intensity in the northern North Atlantic under high (left) and low (right) NAO conditions. Blue (magenta) solid

arrows indicate the upper-ocean flows with higher fraction of colder fresher subpolar (warmer saltier subtropical) waters. The main pathways of the Nordic overflow-derived deep waters are shown with the dotted curves. "C" and "E" symbols are used to denote, respectively, the deep convection sites and the domain, where the Atlantic waters are entrained into ISOW. Larger (smaller) circles indicate stronger (weaker) convection. SPG and STG – the subpolar and subtropical gyres, respectively. Adapted from [Sarafanov, 2009].

Fig. 8. The Deep Western Boundary Current (DWBC) transport variability and its link to the convection intensity in the Labrador Sea. **(a)** Locations of the hydrographic sections (1991–2007) and schematic of the deep water circulation in the Irminger Sea. **(b)** The DWBC transport anomalies at Cape Farewell in 1991–2007, 1 Sv = 10^6 m^3 s^{-1}. The 1994–1997 and 2000–2007 mean anomalies and the 1994–2007 linear trend are shown. **(c)** Anomalies of the DWBC transport at Cape Farewell and the Labrador Sea Water (LSW) thickness in the Labrador Sea in the 1950s–2000s. **(d)** Correlation coefficient (R^2) for the two times series shown in **(c)** at the 0–5-year lag, the LSW thickness leads. The correlation maximum is achieved at the 1–3-year lag. The DWBC transport anomalies in the southern Irminger Sea are foregone by the convection intensity anomalies in the Labrador Sea. Adapted from [Sarafanov et al., 2009].

Fig. 9. Schematic diagram of the Meridional Overturning Circulation (MOC) at the northern periphery of the Atlantic Ocean, northeast of Cape Farewell. The dotted lines refer to the σ_0 isopycnals 27.55 and 27.80. The arrows denote the integral meridional and diapycnal volume fluxes. Where the signs are specified, the positive (negative) transports are northward (southward). The NAC and EGIC transports in the upper layer ($\sigma_0 < 27.55$) at 59.5°N are the throughputs accounting for the recirculations. EGIC – the East Greenland / Irminger Current – refers to the upper part of the Western Boundary Current. Other abbreviations are explained in the legend to **Fig. 3**. Adapted from [Sarafanov et al., 2012].

Fig. 10. Salinity observed in the northwestern Irminger Sea at 64.3°N in February 1998. The σ_0 isopycnals 27.55, 27.70, 27.80 and 27.88 are plotted as the thick black lines; the station locations are marked with the ticks on the top axis. The plot shows fresh dense waters descending (cascading) down the continental slope of Greenland down to the LSW layer ($27.70 < \sigma_0 < 27.80$) and the layer of the Nordic Seas overflow-derived deep waters ($\sigma_0 > 27.80$). Adapted from [Falina et al., 2012].

Fig. 11. One One-hour averaged atmospheric pressure (mb) measured during 49 cruise of Akademik Ioffe.

Fig. 12. One-hour air temerature (°C) measured during 49 cruise of Akademik Ioffe.

R/V AK. IOFFE CRUISE 49 **Table 1**

CLIVAR UTC POSITION

Station	Cast	Type	Date	Time	Pos	Latitude	Longitude	Nav	Depth	Depth above bottom	N Btl	Comments
3330	1	ROS	061615	0537	BE	59 30.0 N	004 35.2 W	GPS	1123	5	8	CTD,LADCP,O2,SiO3,PO4
3330	1	ROS	061613	2227	BO	59 30.1 N	007 59.8 W	GPS	1123	5	8	CTD,LADCP,O2,SiO3,PO4
3330	1	ROS	061613	2303	EN	59 30.2 N	008 00.0 W	GPS	1123	5	8	CTD,LADCP,O2,SiO3,PO4
3331	1	ROS	061615	0843	BE	59 30.0 N	005 17.8 W	GPS	108	3	8	CTD,LADCP,O2,SiO3,PO4
3331	1	ROS	061613	0852	BO	59 30.0 N	005 18.0 W	GPS	108	3	8	CTD,LADCP,O2,SiO3,PO4
3331	1	ROS	061613	0901	EN	59 30.0 N	005 18.0 W	GPS	108	3	8	CTD,LADCP,O2,SiO3,PO4
3332	1	ROS	061615	1134	BE	59 30.0 N	005 59.9 W	GPS	135	4	18	CTD,LADCP,O2,SiO3,PO4
3332	1	ROS	061613	1145	BO	59 30.1 N	006 00.2 W	GPS	135	4	18	CTD,LADCP,O2,SiO3,PO4
3332	1	ROS	061613	1155	EN	59 30.1 N	006 00.1 W	GPS	135	4	18	CTD,LADCP,O2,SiO3,PO4
3333	1	ROS	061615	1423	BE	59 30.0 N	006 39.9 W	GPS	573	4	15	CTD,LADCP,O2,SiO3,PO4
3333	1	ROS	061613	1437	BO	59 30.1 N	006 40.0 W	GPS	573	4	15	CTD,LADCP,O2,SiO3,PO4
3333	1	ROS	061613	1500	EN	59 30.2 N	006 39.9 W	GPS	573	4	15	CTD,LADCP,O2,SiO3,PO4
3334	1	ROS	061615	1804	BE	59 30.0 N	007 19.4 W	GPS	1062	5	21	CTD,LADCP,O2,SiO3,PO4
3334	1	ROS	061613	1835	BO	59 30.1 N	007 19.6 W	GPS	1062	5	21	CTD,LADCP,O2,SiO3,PO4
3334	1	ROS	061613	1908	EN	59 30.1 N	007 19.3 W	GPS	1062	5	21	CTD,LADCP,O2,SiO3,PO4
3335	1	ROS	061615	2159	BE	59 30.0 N	007 59.3 W	GPS	1123	5	18	CTD,LADCP,O2,SiO3,PO4
3335	1	ROS	061613	2227	BO	59 30.1 N	007 59.8 W	GPS	1123	5	18	CTD,LADCP,O2,SiO3,PO4
3335	1	ROS	061613	2303	EN	59 30.2 N	008 00.0 W	GPS	1123	5	18	CTD,LADCP,O2,SiO3,PO4
3336	1	ROS	061715	0226	BE	59 30.0 N	008 39.9 W	GPS	1378	4	21	CTD,LADCP,O2,SiO3,PO4
3336	1	ROS	061713	0256	BO	59 30.0 N	008 39.8 W	GPS	1378	4	21	CTD,LADCP,O2,SiO3,PO4
3336	1	ROS	061713	0339	EN	59 29.8 N	008 39.3 W	GPS	1378	4	21	CTD,LADCP,O2,SiO3,PO4
3337	1	ROS	061715	0632	BE	59 29.9 N	009 19.6 W	GPS	1466	3	21	CTD,LADCP,O2,SiO3,PO4
3337	1	ROS	061713	0706	BO	59 30.2 N	009 19.7 W	GPS	1466	3	21	CTD,LADCP,O2,SiO3,PO4
3337	1	ROS	061713	0748	EN	59 30.5 N	009 19.1 W	GPS	1466	3	21	CTD,LADCP,O2,SiO3,PO4
3338	1	ROS	061715	1040	BE	59 30.0 N	009 59.5 W	GPS	1024	5	21	CTD,LADCP,O2,SiO3,PO4
3338	1	ROS	061713	1110	BO	59 30.0 N	009 59.7 W	GPS	1024	5	21	CTD,LADCP,O2,SiO3,PO4
3338	1	ROS	061713	1147	EN	59 30.0 N	009 59.0 W	GPS	1024	5	21	CTD,LADCP,O2,SiO3,PO4
3339	1	ROS	061715	1456	BE	59 30.0 N	010 39.7 W	GPS	1519	2	21	CTD,LADCP,O2,SiO3,PO4

3339	1	ROS	061713	1530	BO	59 30.2 N	010 39.6 W	GPS	1519	2	21	CTD,LADCP,O2,SiO3,PO4
3339	1	ROS	061713	1612	EN	59 30.2 N	010 38.8 W	GPS	1519	2	21	CTD,LADCP,O2,SiO3,PO4
3340	1	ROS	061715	1942	BE	59 29.9 N	011 19.6 W	GPS	1613	6	21	CTD,LADCP,O2,SiO3,PO4
3340	1	ROS	061713	2021	BO	59 30.0 N	011 19.5 W	GPS	1613	6	21	CTD,LADCP,O2,SiO3,PO4
3340	1	ROS	061713	2108	EN	59 30.0 N	011 19.7 W	GPS	1613	6	21	CTD,LADCP,O2,SiO3,PO4
3341	1	ROS	061815	0104	BE	59 29.9 N	011 59.8 W	GPS	1500	8	19	CTD,LADCP,O2,SiO3,PO4
3341	1	ROS	061813	0134	BO	59 29.9 N	011 59.9 W	GPS	1500	8	19	CTD,LADCP,O2,SiO3,PO4
3341	1	ROS	061813	0220	EN	59 29.8 N	011 59.9 W	GPS	1500	8	19	CTD,LADCP,O2,SiO3,PO4
3342	1	ROS	061815	0723	BE	59 30.0 N	012 59.4 W	GPS	1293	7	21	CTD,LADCP,O2,SiO3,PO4
3342	1	ROS	061813	0756	BO	59 30.1 N	012 59.7 W	GPS	1293	7	21	CTD,LADCP,O2,SiO3,PO4
3342	1	ROS	061813	0841	EN	59 30.3 N	012 58.9 W	GPS	1293	7	21	CTD,LADCP,O2,SiO3,PO4
3343	1	ROS	061815	1324	BE	59 29.9 N	013 59.7 W	GPS	989	5	20	CTD,LADCP,O2,SiO3,PO4
3343	1	ROS	061813	1349	BO	59 29.8 N	014 00.1 W	GPS	989	5	20	CTD,LADCP,O2,SiO3,PO4
3343	1	ROS	061813	1419	EN	59 29.7 N	014 00.3 W	GPS	989	5	20	CTD,LADCP,O2,SiO3,PO4
3344	1	ROS	061815	1857	BE	59 29.9 N	014 59.7 W	GPS	1411	5	21	CTD,LADCP,O2,SiO3,PO4
3344	1	ROS	061813	1929	BO	59 30.0 N	014 59.5 W	GPS	1411	5	21	CTD,LADCP,O2,SiO3,PO4
3344	1	ROS	061813	2012	EN	59 30.0 N	014 59.0 W	GPS	1411	5	21	CTD,LADCP,O2,SiO3,PO4
3345	1	ROS	061915	0025	BE	59 30.0 N	015 59.8 W	GPS	1538	4	21	CTD,LADCP,O2,SiO3,PO4
3345	1	ROS	061913	0058	BO	59 30.0 N	016 00.0 W	GPS	1538	4	21	CTD,LADCP,O2,SiO3,PO4
3345	1	ROS	061913	0151	EN	59 30.0 N	016 00.0 W	GPS	1538	4	21	CTD,LADCP,O2,SiO3,PO4
3346	1	ROS	061915	0538	BE	59 30.0 N	016 59.8 W	GPS	1227	4	21	CTD,LADCP,O2,SiO3,PO4
3346	1	ROS	061913	0608	BO	59 29.9 N	016 59.7 W	GPS	1227	4	21	CTD,LADCP,O2,SiO3,PO4
3346	1	ROS	061913	0650	EN	59 30.0 N	016 59.8 W	GPS	1227	4	21	CTD,LADCP,O2,SiO3,PO4
3347	1	ROS	061915	0843	BE	59 30.0 N	017 29.6 W	GPS	1919	5	21	CTD,LADCP,O2,SiO3,PO4
3347	1	ROS	061913	0922	BO	59 30.3 N	017 29.6 W	GPS	1919	5	21	CTD,LADCP,O2,SiO3,PO4
3347	1	ROS	061913	1009	EN	59 30.7 N	017 29.5 W	GPS	1919	5	21	CTD,LADCP,O2,SiO3,PO4
3348	1	ROS	061915	1207	BE	59 30.0 N	017 59.7 W	GPS	2183	5	21	CTD,LADCP,O2,SiO3,PO4
3348	1	ROS	061913	1251	BO	59 30.0 N	017 59.9 W	GPS	2183	5	21	CTD,LADCP,O2,SiO3,PO4
3348	1	ROS	061913	1348	EN	59 30.0 N	017 59.9 W	GPS	2183	5	21	CTD,LADCP,O2,SiO3,PO4
3348a	1	ROS	061915	1443	BE	59 30.0 N	017 59.9 W	GPS	2186	4	20	Suspended sediment matter
3348a	1	ROS	061913	1529	BO	59 30.0 N	017 59.9 W	GPS	2186	4	20	Suspended sediment matter
3348a	1	ROS	061913	1612	EN	59 30.0 N	017 59.9 W	GPS	2186	4	20	Suspended sediment matter
3349	1	ROS	061915	2128	BE	59 30.0 N	018 39.8 W	GPS	2775	6	21	CTD,LADCP,O2,SiO3,PO4

3349	1	ROS	061913	2221	BO	59 30.4 N	018 39.4 W	GPS	2775	6	21	CTD,LADCP,O2,SiO3,PO4
3349	1	ROS	061913	2329	EN	59 30.8 N	018 38.6 W	GPS	2775	6	21	CTD,LADCP,O2,SiO3,PO4
3350	1	ROS	062015	0213	BE	59 30.0 N	019 19.9 W	GPS	2702	5	21	CTD,LADCP,O2,SiO3,PO4
3350	1	ROS	062013	0304	BO	59 29.8 N	019 19.3 W	GPS	2702	5	21	CTD,LADCP,O2,SiO3,PO4
3350	1	ROS	062013	0407	EN	59 29.5 N	019 18.9 W	GPS	2702	5	21	CTD,LADCP,O2,SiO3,PO4
3351	1	ROS	062015	0651	BE	59 30.0 N	019 59.7 W	GPS	2762	5	21	CTD,LADCP,O2,SiO3,PO4
3351	1	ROS	062013	0747	BO	59 29.3 N	019 59.3 W	GPS	2762	5	21	CTD,LADCP,O2,SiO3,PO4
3351	1	ROS	062013	0851	EN	59 28.6 N	019 58.9 W	GPS	2762	5	21	CTD,LADCP,O2,SiO3,PO4
3352	1	ROS	062015	1159	BE	59 30.0 N	020 39.5 W	GPS	2822	2	21	CTD,LADCP,O2,SiO3,PO4
3352	1	ROS	062013	1256	BO	59 30.1 N	020 39.3 W	GPS	2822	2	21	CTD,LADCP,O2,SiO3,PO4
3352	1	ROS	062013	1404	EN	59 30.0 N	020 38.3 W	GPS	2822	2	21	CTD,LADCP,O2,SiO3,PO4
3352a	1	ROS	062015	1507	BE	59 30.0 N	020 37.2 W	GPS	2822	4	21	Suspended sediment matter
3352a	1	ROS	062013	1603	BO	59 30.0 N	020 36.2 W	GPS	2822	4	21	Suspended sediment matter
3352a	1	ROS	062013	1655	EN	59 29.9 N	020 35.3 W	GPS	2822	4	21	Suspended sediment matter
3353	1	ROS	062015	1947	BE	59 30.0 N	021 19.8 W	GPS	2854	4	21	CTD,LADCP,O2,SiO3,PO4
3353	1	ROS	062013	2044	BO	59 30.2 N	021 19.8 W	GPS	2854	4	21	CTD,LADCP,O2,SiO3,PO4
3353	1	ROS	062013	2149	EN	59 30.0 N	021 19.2 W	GPS	2854	4	21	CTD,LADCP,O2,SiO3,PO4
3354	1	ROS	062115	0027	BE	59 30.0 N	022 00.0 W	GPS	2738	5	21	CTD,LADCP,O2,SiO3,PO4
3354	1	ROS	062113	0118	BO	59 30.0 N	021 59.9 W	GPS	2738	5	21	CTD,LADCP,O2,SiO3,PO4
3354	1	ROS	062113	0221	EN	59 29.8 N	021 59.8 W	GPS	2738	5	21	CTD,LADCP,O2,SiO3,PO4
3355	1	ROS	062115	0459	BE	59 29.9 N	022 39.8 W	GPS	2455	4	21	CTD,LADCP,O2,SiO3,PO4
3355	1	ROS	062113	0549	BO	59 30.0 N	022 39.6 W	GPS	2455	4	21	CTD,LADCP,O2,SiO3,PO4
3355	1	ROS	062113	0645	EN	59 30.0 N	022 39.3 W	GPS	2455	4	21	CTD,LADCP,O2,SiO3,PO4
3356	1	ROS	062115	0911	BE	59 30.0 N	023 19.5 W	GPS	2428	7	21	CTD,LADCP,O2,SiO3,PO4
3356	1	ROS	062113	1001	BO	59 29.8 N	023 20.1 W	GPS	2428	7	21	CTD,LADCP,O2,SiO3,PO4
3356	1	ROS	062113	1055	EN	59 29.9 N	023 20.2 W	GPS	2428	7	21	CTD,LADCP,O2,SiO3,PO4
3357	1	ROS	062115	1314	BE	59 29.9 N	023 59.7 W	GPS	2515	4	21	CTD,LADCP,O2,SiO3,PO4
3357	1	ROS	062113	1404	BO	59 29.8 N	023 59.9 W	GPS	2515	4	21	CTD,LADCP,O2,SiO3,PO4
3357	1	ROS	062113	1459	EN	59 29.8 N	023 59.8 W	GPS	2515	4	21	CTD,LADCP,O2,SiO3,PO4
3358	1	ROS	062115	1617	BE	59 30.0 N	024 19.6 W	GPS	2653	4	21	CTD,LADCP,O2,SiO3,PO4
3358	1	ROS	062113	1711	BO	59 30.1 N	024 20.1 W	GPS	2653	4	21	CTD,LADCP,O2,SiO3,PO4
3358	1	ROS	062113	1809	EN	59 30.1 N	024 20.3 W	GPS	2653	4	21	CTD,LADCP,O2,SiO3,PO4
3359	1	ROS	062115	1926	BE	59 29.9 N	024 39.9 W	GPS	2516	7	21	CTD,LADCP,O2,SiO3,PO4

3359	1	ROS	062113	2015	BO	59 29.9 N	024 40.2 W	GPS	2516	7	21	CTD,LADCP,O2,SiO3,PO4
3359	1	ROS	062113	2113	EN	59 30.0 N	024 40.6 W	GPS	2516	7	21	CTD,LADCP,O2,SiO3,PO4
3359a	1	ROS	062115	2204	BE	59 29.9 N	024 40.9 W	GPS	2546	5	21	Suspended sediment matter
3359a	1	ROS	062113	2251	BO	59 29.9 N	024 41.4 W	GPS	2546	5	21	Suspended sediment matter
3359a	1	ROS	062113	2337	EN	59 29.8 N	024 42.0 W	GPS	2546	5	21	Suspended sediment matter
3360	1	ROS	062215	0350	BE	59 29.9 N	025 00.0 W	GPS	2474	4	21	CTD,LADCP,O2,SiO3,PO4
3360	1	ROS	062213	0437	BO	59 29.9 N	025 00.0 W	GPS	2474	4	21	CTD,LADCP,O2,SiO3,PO4
3360	1	ROS	062213	0540	EN	59 30.0 N	025 00.0 W	GPS	2474	4	21	CTD,LADCP,O2,SiO3,PO4
3361	1	ROS	062215	0651	BE	59 29.9 N	025 19.6 W	GPS	2486	4	20	CTD,LADCP,O2,SiO3,PO4
3361	1	ROS	062213	0741	BO	59 30.0 N	025 20.0 W	GPS	2486	4	20	CTD,LADCP,O2,SiO3,PO4
3361	1	ROS	062213	0835	EN	59 30.0 N	025 19.9 W	GPS	2486	4	20	CTD,LADCP,O2,SiO3,PO4
3362	1	ROS	062215	0950	BE	59 29.9 N	025 39.6 W	GPS	2470	5	21	CTD,LADCP,O2,SiO3,PO4
3362	1	ROS	062213	1041	BO	59 29.9 N	025 40.0 W	GPS	2470	5	21	CTD,LADCP,O2,SiO3,PO4
3362	1	ROS	062213	1140	EN	59 29.9 N	025 40.0 W	GPS	2470	5	21	CTD,LADCP,O2,SiO3,PO4
3363	1	ROS	062215	1255	BE	59 29.9 N	025 59.8 W	GPS	2269	5	21	CTD,LADCP,O2,SiO3,PO4
3363	1	ROS	062213	1342	BO	59 30.0 N	026 00.1 W	GPS	2269	5	21	CTD,LADCP,O2,SiO3,PO4
3363	1	ROS	062213	1433	EN	59 30.0 N	026 00.1 W	GPS	2269	5	21	CTD,LADCP,O2,SiO3,PO4
3364	1	ROS	062215	1546	BE	59 29.9 N	026 19.8 W	GPS	2328	4	21	CTD,LADCP,O2,SiO3,PO4
3364	1	ROS	062213	1634	BO	59 30.2 N	026 20.4 W	GPS	2328	4	21	CTD,LADCP,O2,SiO3,PO4
3364	1	ROS	062213	1727	EN	59 30.5 N	026 20.6 W	GPS	2328	4	21	CTD,LADCP,O2,SiO3,PO4
3365	1	ROS	062215	1838	BE	59 29.9 N	026 39.7 W	GPS	2235	4	21	CTD,LADCP,O2,SiO3,PO4
3365	1	ROS	062213	1923	BO	59 30.0 N	026 39.7 W	GPS	2235	4	21	CTD,LADCP,O2,SiO3,PO4
3365	1	ROS	062213	2019	EN	59 30.2 N	026 39.6 W	GPS	2235	4	21	CTD,LADCP,O2,SiO3,PO4
3366	1	ROS	062215	2241	BE	59 30.0 N	027 19.8 W	GPS	1894	6	21	CTD,LADCP,O2,SiO3,PO4
3366	1	ROS	062213	2316	BO	59 30.2 N	027 19.8 W	GPS	1894	6	21	CTD,LADCP,O2,SiO3,PO4
3366	1	ROS	062313	0007	EN	59 30.3 N	027 19.8 W	GPS	1894	6	21	CTD,LADCP,O2,SiO3,PO4
3367	1	ROS	062315	0232	BE	59 30.0 N	028 00.0 W	GPS	1989	7	21	CTD,LADCP,O2,SiO3,PO4
3367	1	ROS	062313	0311	BO	59 30.2 N	027 59.8 W	GPS	1989	7	21	CTD,LADCP,O2,SiO3,PO4
3367	1	ROS	062313	0402	EN	59 30.3 N	027 59.4 W	GPS	1989	7	21	CTD,LADCP,O2,SiO3,PO4
3368	1	ROS	062315	0624	BE	59 29.9 N	028 39.9 W	GPS	1677	5	20	CTD,LADCP,O2,SiO3,PO4
3368	1	ROS	062313	0706	BO	59 30.0 N	028 40.5 W	GPS	1677	5	20	CTD,LADCP,O2,SiO3,PO4
3368	1	ROS	062313	0746	EN	59 29.8 N	028 40.7 W	GPS	1677	5	20	CTD,LADCP,O2,SiO3,PO4
3369	1	ROS	062315	0958	BE	59 29.9 N	029 20.0 W	GPS	1416	5	20	CTD,LADCP,O2,SiO3,PO4

3369	1	ROS	062313	1028	BO	59 29.9 N	029 19.9 W	GPS	1416	5	20	CTD,LADCP,O2,SiO3,PO4
3369	1	ROS	062313	1107	EN	59 30.0 N	029 19.8 W	GPS	1416	5	20	CTD,LADCP,O2,SiO3,PO4
3370	1	ROS	062315	1326	BE	59 29.9 N	030 00.3 W	GPS	1473	5	20	CTD,LADCP,O2,SiO3,PO4
3370	1	ROS	062313	1358	BO	59 30.2 N	030 00.0 W	GPS	1473	5	20	CTD,LADCP,O2,SiO3,PO4
3370	1	ROS	062313	1438	EN	59 30.4 N	029 59.9 W	GPS	1473	5	20	CTD,LADCP,O2,SiO3,PO4
3371	1	ROS	062315	1550	BE	59 29.8 N	030 20.2 W	GPS	1345	5	21	CTD,LADCP,O2,SiO3,PO4
3371	1	ROS	062313	1622	BO	59 29.8 N	030 20.0 W	GPS	1345	5	21	CTD,LADCP,O2,SiO3,PO4
3371	1	ROS	062313	1701	EN	59 29.8 N	030 20.0 W	GPS	1345	5	21	CTD,LADCP,O2,SiO3,PO4
3372	1	ROS	062315	1815	BE	59 30.0 N	030 40.0 W	GPS	1529	7	21	CTD,LADCP,O2,SiO3,PO4
3372	1	ROS	062313	1844	BO	59 30.0 N	030 39.9 W	GPS	1529	7	21	CTD,LADCP,O2,SiO3,PO4
3372	1	ROS	062313	1930	EN	59 30.1 N	030 39.9 W	GPS	1529	7	21	CTD,LADCP,O2,SiO3,PO4
3373	1	ROS	062315	2046	BE	59 30.0 N	030 59.9 W	GPS	1543	5	21	CTD,LADCP,O2,SiO3,PO4
3373	1	ROS	062313	2115	BO	59 30.1 N	030 59.9 W	GPS	1543	5	21	CTD,LADCP,O2,SiO3,PO4
3373	1	ROS	062313	2201	EN	59 30.4 N	031 00.0 W	GPS	1543	5	21	CTD,LADCP,O2,SiO3,PO4
3374	1	ROS	062315	2318	BE	59 30.0 N	031 20.0 W	GPS	1754	4	21	CTD,LADCP,O2,SiO3,PO4
3374	1	ROS	062313	2351	BO	59 30.1 N	031 20.2 W	GPS	1754	4	21	CTD,LADCP,O2,SiO3,PO4
3374	1	ROS	062413	0040	EN	59 30.4 N	031 20.6 W	GPS	1754	4	21	CTD,LADCP,O2,SiO3,PO4
3375	1	ROS	062415	0157	BE	59 29.9 N	031 40.0 W	GPS	1904	4	19	CTD,LADCP,O2,SiO3,PO4
3375	1	ROS	062413	0237	BO	59 30.0 N	031 39.9 W	GPS	1904	4	19	CTD,LADCP,O2,SiO3,PO4
3375	1	ROS	062413	0330	EN	59 30.0 N	031 39.8 W	GPS	1904	4	19	CTD,LADCP,O2,SiO3,PO4
3376	1	ROS	062415	0452	BE	59 30.0 N	032 00.1 W	GPS	1920	4	21	CTD,LADCP,O2,SiO3,PO4
3376	1	ROS	062413	0533	BO	59 30.0 N	031 59.9 W	GPS	1920	4	21	CTD,LADCP,O2,SiO3,PO4
3376	1	ROS	062413	0623	EN	59 29.9 N	031 59.8 W	GPS	1920	4	21	CTD,LADCP,O2,SiO3,PO4
3377	1	ROS	062415	0756	BE	59 29.8 N	032 25.3 W	GPS	2137	4	21	CTD,LADCP,O2,SiO3,PO4
3377	1	ROS	062413	0847	BO	59 30.0 N	032 25.1 W	GPS	2137	4	21	CTD,LADCP,O2,SiO3,PO4
3377	1	ROS	062413	0940	EN	59 30.2 N	032 24.9 W	GPS	2137	4	21	CTD,LADCP,O2,SiO3,PO4
3378	1	ROS	062415	1124	BE	59 30.0 N	032 50.9 W	GPS	2176	7	21	CTD,LADCP,O2,SiO3,PO4
3378	1	ROS	062413	1207	BO	59 30.0 N	032 50.7 W	GPS	2176	7	21	CTD,LADCP,O2,SiO3,PO4
3378	1	ROS	062413	1259	EN	59 30.0 N	032 50.5 W	GPS	2176	7	21	CTD,LADCP,O2,SiO3,PO4
3378a	1	ROS	062415	1349	BE	59 30.0 N	032 50.6 W	GPS	2193	4	21	Suspended sediment matter
3378a	1	ROS	062413	1431	BO	59 30.1 N	032 50.5 W	GPS	2193	4	21	Suspended sediment matter
3378a	1	ROS	062413	1511	EN	59 30.2 N	032 50.5 W	GPS	2193	4	21	Suspended sediment matter
3379	1	ROS	062415	1933	BE	59 30.0 N	033 20.0 W	GPS	2187	5	20	CTD,LADCP,O2,SiO3,PO4

3379	1	ROS	062413	2014	BO	59 30.0 N	033 20.1 W	GPS	2187	5	20	CTD,LADCP,O2,SiO3,PO4
3379	1	ROS	062413	2114	EN	59 30.2 N	033 20.2 W	GPS	2187	5	20	CTD,LADCP,O2,SiO3,PO4
3380	1	ROS	062415	2330	BE	59 29.9 N	034 00.0 W	GPS	2615	6	21	CTD,LADCP,O2,SiO3,PO4
3380	1	ROS	062513	0020	BO	59 30.1 N	034 00.2 W	GPS	2615	6	21	CTD,LADCP,O2,SiO3,PO4
3380	1	ROS	062513	0123	EN	59 30.3 N	034 00.5 W	GPS	2615	6	21	CTD,LADCP,O2,SiO3,PO4
3381	1	ROS	062515	0346	BE	59 29.9 N	034 40.0 W	GPS	2809	4	21	CTD,LADCP,O2,SiO3,PO4
3381	1	ROS	062513	0440	BO	59 30.0 N	034 40.5 W	GPS	2809	4	21	CTD,LADCP,O2,SiO3,PO4
3381	1	ROS	062513	0549	EN	59 30.0 N	034 41.3 W	GPS	2809	4	21	CTD,LADCP,O2,SiO3,PO4
3382	1	ROS	062515	0805	BE	59 30.0 N	035 20.1 W	GPS	1951	4	21	CTD,LADCP,O2,SiO3,PO4
3382	1	ROS	062513	0846	BO	59 30.0 N	035 20.1 W	GPS	1951	4	21	CTD,LADCP,O2,SiO3,PO4
3382	1	ROS	062513	0934	EN	59 30.0 N	035 19.8 W	GPS	1951	4	21	CTD,LADCP,O2,SiO3,PO4
3383	1	ROS	062515	1210	BE	59 29.8 N	036 05.9 W	GPS	3084	4	21	CTD,LADCP,O2,SiO3,PO4
3383	1	ROS	062513	1310	BO	59 29.6 N	036 06.7 W	GPS	3084	4	21	CTD,LADCP,O2,SiO3,PO4
3383	1	ROS	062513	1418	EN	59 29.2 N	036 07.5 W	GPS	3084	4	21	CTD,LADCP,O2,SiO3,PO4
3383a	1	ROS	062515	1530	BE	59 28.7 N	036 08.5 W	GPS	3085	6	21	Suspended sediment matter
3383a	1	ROS	062513	1627	BO	59 28.4 N	036 09.1 W	GPS	3085	6	21	Suspended sediment matter
3383a	1	ROS	062513	1723	EN	59 28.0 N	036 09.5 W	GPS	3085	6	21	Suspended sediment matter
3384	1	ROS	062515	2030	BE	59 29.9 N	036 40.0 W	GPS	3097	4	21	CTD,LADCP,O2,SiO3,PO4
3384	1	ROS	062513	2129	BO	59 29.7 N	036 40.4 W	GPS	3097	4	21	CTD,LADCP,O2,SiO3,PO4
3384	1	ROS	062513	2247	EN	59 29.3 N	036 40.8 W	GPS	3097	4	21	CTD,LADCP,O2,SiO3,PO4
3385	1	ROS	062615	0108	BE	59 30.1 N	037 19.4 W	GPS	3204	7	21	CTD,LADCP,O2,SiO3,PO4
3385	1	ROS	062613	0206	BO	59 30.1 N	037 20.2 W	GPS	3204	7	21	CTD,LADCP,O2,SiO3,PO4
3385	1	ROS	062613	0325	EN	59 30.2 N	037 21.3 W	GPS	3204	7	21	CTD,LADCP,O2,SiO3,PO4
3386	1	ROS	062615	0608	BE	59 29.8 N	037 59.8 W	GPS	3111	3	21	CTD,LADCP,O2,SiO3,PO4
3386	1	ROS	062613	0709	BO	59 30.4 N	037 59.8 W	GPS	3111	3	21	CTD,LADCP,O2,SiO3,PO4
3386	1	ROS	062613	0819	EN	59 31.0 N	037 59.6 W	GPS	3111	3	21	CTD,LADCP,O2,SiO3,PO4
3387	1	ROS	062615	1047	BE	59 29.8 N	038 40.1 W	GPS	2996	4	21	CTD,LADCP,O2,SiO3,PO4
3387	1	ROS	062613	1149	BO	59 29.4 N	038 39.4 W	GPS	2996	4	21	CTD,LADCP,O2,SiO3,PO4
3387	1	ROS	062613	1255	EN	59 28.8 N	038 38.8 W	GPS	2996	4	21	CTD,LADCP,O2,SiO3,PO4
3388	1	ROS	062615	1524	BE	59 29.7 N	039 19.9 W	GPS	2922	2	21	CTD,LADCP,O2,SiO3,PO4
3388	1	ROS	062613	1625	BO	59 29.9 N	039 20.1 W	GPS	2922	2	21	CTD,LADCP,O2,SiO3,PO4
3388	1	ROS	062613	1731	EN	59 29.6 N	039 20.3 W	GPS	2922	2	21	CTD,LADCP,O2,SiO3,PO4
3389	1	ROS	062615	2008	BE	59 30.0 N	040 00.1 W	GPS	2889	3	21	CTD,LADCP,O2,SiO3,PO4

3389	1	ROS	062613	2102	BO	59 29.9 N	039 59.9 W	GPS	2889	3	21	CTD,LADCP,O2,SiO3,PO4
3389	1	ROS	062613	2206	EN	59 29.9 N	039 59.8 W	GPS	2889	3	21	CTD,LADCP,O2,SiO3,PO4
3390	1	ROS	062615	2325	BE	59 30.0 N	040 19.9 W	GPS	2665	4	21	CTD,LADCP,O2,SiO3,PO4
3390	1	ROS	062713	0014	BO	59 30.2 N	040 20.0 W	GPS	2665	4	21	CTD,LADCP,O2,SiO3,PO4
3390	1	ROS	062713	0118	EN	59 30.6 N	040 20.1 W	GPS	2665	4	21	CTD,LADCP,O2,SiO3,PO4
3391	1	ROS	062715	0243	BE	59 29.9 N	040 39.9 W	GPS	2580	4	21	CTD,LADCP,O2,SiO3,PO4
3391	1	ROS	062713	0332	BO	59 30.0 N	040 39.9 W	GPS	2580	4	21	CTD,LADCP,O2,SiO3,PO4
3391	1	ROS	062713	0437	EN	59 29.9 N	040 40.0 W	GPS	2580	4	21	CTD,LADCP,O2,SiO3,PO4
3392	1	ROS	062715	0640	BE	59 33.8 N	040 59.9 W	GPS	2396	3	21	CTD,LADCP,O2,SiO3,PO4
3392	1	ROS	062713	0728	BO	59 33.9 N	041 00.1 W	GPS	2396	3	21	CTD,LADCP,O2,SiO3,PO4
3392	1	ROS	062713	0823	EN	59 33.8 N	041 00.1 W	GPS	2396	3	21	CTD,LADCP,O2,SiO3,PO4
3393	1	ROS	062715	0937	BE	59 38.5 N	041 16.2 W	GPS	2202	4	21	CTD,LADCP,O2,SiO3,PO4
3393	1	ROS	062713	1019	BO	59 38.4 N	041 15.8 W	GPS	2202	4	21	CTD,LADCP,O2,SiO3,PO4
3393	1	ROS	062713	1112	EN	59 38.1 N	041 15.7 W	GPS	2202	4	21	CTD,LADCP,O2,SiO3,PO4
3394	1	ROS	062715	1225	BE	59 42.4 N	041 32.0 W	GPS	1990	3	21	CTD,LADCP,O2,SiO3,PO4
3394	1	ROS	062713	1303	BO	59 42.3 N	041 32.4 W	GPS	1990	3	21	CTD,LADCP,O2,SiO3,PO4
3394	1	ROS	062713	1354	EN	59 41.9 N	041 32.9 W	GPS	1990	3	21	CTD,LADCP,O2,SiO3,PO4
3395	1	ROS	062715	1504	BE	59 46.4 N	041 46.9 W	GPS	1828	3	20	CTD,LADCP,O2,SiO3,PO4
3395	1	ROS	062713	1542	BO	59 46.5 N	041 47.5 W	GPS	1828	3	20	CTD,LADCP,O2,SiO3,PO4
3395	1	ROS	062713	1629	EN	59 46.5 N	041 48.0 W	GPS	1828	3	20	CTD,LADCP,O2,SiO3,PO4
3396	1	ROS	062715	1710	BE	59 48.5 N	041 55.5 W	GPS	1754	4	21	CTD,LADCP,O2,SiO3,PO4
3396	1	ROS	062713	1746	BO	59 48.5 N	041 56.4 W	GPS	1754	4	21	CTD,LADCP,O2,SiO3,PO4
3396	1	ROS	062713	1834	EN	59 48.1 N	041 57.7 W	GPS	1754	4	21	CTD,LADCP,O2,SiO3,PO4
3397	1	ROS	062715	1915	BE	59 50.7 N	042 03.3 W	GPS	1633	4	21	CTD,LADCP,O2,SiO3,PO4
3397	1	ROS	062713	1949	BO	59 50.3 N	042 04.2 W	GPS	1633	4	21	CTD,LADCP,O2,SiO3,PO4
3397	1	ROS	062713	2036	EN	59 49.8 N	042 05.0 W	GPS	1633	4	21	CTD,LADCP,O2,SiO3,PO4
3398	1	ROS	062715	2112	BE	59 51.4 N	042 06.5 W	GPS	1555	3	18	CTD,LADCP,O2,SiO3,PO4
3398	1	ROS	062713	2142	BO	59 51.1 N	042 07.0 W	GPS	1555	3	18	CTD,LADCP,O2,SiO3,PO4
3398	1	ROS	062713	2225	EN	59 50.6 N	042 07.6 W	GPS	1555	3	18	CTD,LADCP,O2,SiO3,PO4
3399	1	ROS	062715	2255	BE	59 52.2 N	042 09.1 W	GPS	1424	3	17	CTD,LADCP,O2,SiO3,PO4
3399	1	ROS	062713	2324	BO	59 52.0 N	042 09.7 W	GPS	1424	3	17	CTD,LADCP,O2,SiO3,PO4
3399	1	ROS	062813	0003	EN	59 51.7 N	042 10.7 W	GPS	1424	3	17	CTD,LADCP,O2,SiO3,PO4
3400	1	ROS	062815	0033	BE	59 52.9 N	042 12.2 W	GPS	810	2	16	CTD,LADCP,O2,SiO3,PO4

3400	1	ROS	062813	0051	BO	59 52.8 N	042 12.4 W	GPS	810	2	16	CTD,LADCP,O2,SiO3,PO4
3400	1	ROS	062813	0120	EN	59 52.6 N	042 12.8 W	GPS	810	2	16	CTD,LADCP,O2,SiO3,PO4
3401	1	ROS	062815	0145	BE	59 53.3 N	042 15.4 W	GPS	381	4	9	CTD,LADCP,O2,SiO3,PO4
3401	1	ROS	062813	0200	BO	59 53.3 N	042 15.6 W	GPS	381	4	9	CTD,LADCP,O2,SiO3,PO4
3401	1	ROS	062813	0214	EN	59 53.3 N	042 15.7 W	GPS	381	4	9	CTD,LADCP,O2,SiO3,PO4
3402	1	ROS	062815	0244	BE	59 54.0 N	042 19.1 W	GPS	322	5	9	CTD,LADCP,O2,SiO3,PO4
3402	1	ROS	062813	0255	BO	59 53.9 N	042 19.3 W	GPS	322	5	9	CTD,LADCP,O2,SiO3,PO4
3402	1	ROS	062813	0309	EN	59 53.9 N	042 19.3 W	GPS	322	5	9	CTD,LADCP,O2,SiO3,PO4
3403	1	ROS	062815	0337	BE	59 54.1 N	042 22.7 W	GPS	228	5	8	CTD,LADCP,O2,SiO3,PO4
3403	1	ROS	062813	0346	BO	59 54.0 N	042 23.0 W	GPS	228	5	8	CTD,LADCP,O2,SiO3,PO4
3403	1	ROS	062813	0358	EN	59 53.9 N	042 23.1 W	GPS	228	5	8	CTD,LADCP,O2,SiO3,PO4
3404	1	ROS	062815	0421	BE	59 54.2 N	042 26.3 W	GPS	214	5	9	CTD,LADCP,O2,SiO3,PO4
3404	1	ROS	062813	0435	BO	59 54.2 N	042 26.7 W	GPS	214	5	9	CTD,LADCP,O2,SiO3,PO4
3404	1	ROS	062813	0447	EN	59 54.0 N	042 27.1 W	GPS	214	5	9	CTD,LADCP,O2,SiO3,PO4
3405	1	ROS	062815	0508	BE	59 54.5 N	042 29.9 W	GPS	199	5	7	CTD,LADCP,O2,SiO3,PO4
3405	1	ROS	062813	0519	BO	59 54.4 N	042 30.2 W	GPS	199	5	7	CTD,LADCP,O2,SiO3,PO4
3405	1	ROS	062813	0530	EN	59 54.3 N	042 30.6 W	GPS	199	5	7	CTD,LADCP,O2,SiO3,PO4
3406	1	ROS	062815	0549	BE	59 54.7 N	042 33.5 W	GPS	183	4		
3406	1	ROS	062813	0600	BO	59 54.6 N	042 33.8 W	GPS	183	4		
3406	1	ROS	062813	0604	EN	59 54.6 N	042 33.9 W	GPS	183	4		
3406a	1	ROS	062815	0605	BE	59 54.6 N	042 33.9 W	GPS	183	1	10	CTD,LADCP,O2,SiO3,PO4
3406a	1	ROS	062813	0610	BO	59 54.5 N	042 33.9 W	GPS	183	1	10	CTD,LADCP,O2,SiO3,PO4
3406a	1	ROS	062813	0622	EN	59 54.2 N	042 33.9 W	GPS	183	1	10	CTD,LADCP,O2,SiO3,PO4
3407	1	ROS	062815	0646	BE	59 55.1 N	042 37.1 W	GPS	181	4	7	CTD,LADCP,O2,SiO3,PO4
3407	1	ROS	062813	0654	BO	59 55.0 N	042 37.3 W	GPS	181	4	7	CTD,LADCP,O2,SiO3,PO4
3407	1	ROS	062813	0704	EN	59 54.9 N	042 37.5 W	GPS	181	4	7	CTD,LADCP,O2,SiO3,PO4
3408	1	ROS	062815	0724	BE	59 55.5 N	042 40.7 W	GPS	185	2	7	CTD,LADCP,O2,SiO3,PO4
3408	1	ROS	062813	0734	BO	59 55.5 N	042 41.1 W	GPS	185	2	7	CTD,LADCP,O2,SiO3,PO4
3408	1	ROS	062813	0744	EN	59 55.4 N	042 41.3 W	GPS	185	2	7	CTD,LADCP,O2,SiO3,PO4
3409	1	ROS	062815	0759	BE	59 55.6 N	042 44.3 W	GPS	188	4		
3409	1	ROS	062813	0810	BO	59 55.6 N	042 44.7 W	GPS	188	4		
3409	1	ROS	062813	0819	EN	59 55.5 N	042 44.7 W	GPS	188	4		
3410	1	ROS	062815	0838	BE	59 56.1 N	042 47.8 W	GPS	180	3	6	CTD,LADCP,O2,SiO3,PO4

3410	1	ROS	062813	0847	BO	59 56.1 N	042 48.1 W	GPS	180	3	6	CTD,LADCP,O2,SiO3,PO4
3410	1	ROS	062813	0856	EN	59 56.1 N	042 48.3 W	GPS	180	3	6	CTD,LADCP,O2,SiO3,PO4
3411	1	ROS	062815	0915	BE	59 56.2 N	042 51.7 W	GPS	164	4	6	CTD,LADCP,O2,SiO3,PO4
3411	1	ROS	062813	0923	BO	59 56.2 N	042 51.9 W	GPS	164	4	6	CTD,LADCP,O2,SiO3,PO4
3411	1	ROS	062813	0931	EN	59 56.2 N	042 52.0 W	GPS	164	4	6	CTD,LADCP,O2,SiO3,PO4
3412	1	ROS	062815	0949	BE	59 56.8 N	042 55.1 W	GPS	164	4	6	CTD,LADCP,O2,SiO3,PO4
3412	1	ROS	062813	0957	BO	59 56.9 N	042 55.3 W	GPS	164	4	6	CTD,LADCP,O2,SiO3,PO4
3412	1	ROS	062813	1005	EN	59 56.9 N	042 55.3 W	GPS	164	4	6	CTD,LADCP,O2,SiO3,PO4
3413	1	ROS	062815	1026	BE	59 57.2 N	042 59.2 W	GPS	162	4	6	CTD,LADCP,O2,SiO3,PO4
3413	1	ROS	062813	1034	BO	59 57.3 N	042 59.2 W	GPS	162	4	6	CTD,LADCP,O2,SiO3,PO4
3413	1	ROS	062813	1043	EN	59 57.4 N	042 59.3 W	GPS	162	4	6	CTD,LADCP,O2,SiO3,PO4
3414	1	ROS	062815	1108	BE	59 57.4 N	043 00.5 W	GPS	160	3	10	CTD,LADCP,O2,SiO3,PO4
3414	1	ROS	062813	1120	BO	59 57.4 N	043 00.6 W	GPS	160	3	10	CTD,LADCP,O2,SiO3,PO4
3414	1	ROS	062813	1130	EN	59 57.4 N	043 00.7 W	GPS	160	3	10	CTD,LADCP,O2,SiO3,PO4
3415	1	ROS	062915	1541	BE	55 34.4 N	046 12.4 W	GPS	2985	4	21	CTD,LADCP,O2,SiO3,PO4
3415	1	ROS	062913	1639	BO	55 34.3 N	046 12.5 W	GPS	2985	4	21	CTD,LADCP,O2,SiO3,PO4
3415	1	ROS	062913	1734	EN	55 34.2 N	046 12.7 W	GPS	2985	4	21	CTD,LADCP,O2,SiO3,PO4

Table 2

Station	Date	UTC	Latitude N	Longitude	Depth, m	Sampling
P-1	14.06.2015	8:00	57 ° 45.157 N	07 ° 31.599 E		Water: 0 m
P-2	14.06.2015	18:05	58 ° 09.618 N	05 ° 09.759 E		Water: 0 m
P-3	15.06.2015	7:23	58 ° 58.036 N	01 ° 53.802 E		Water: 0 m
A-1-1	15.06.2015	7:53	58 ° 59.736 N	01 ° 46.155 E		Aerosol nets: beginning
P-4	15.06.2015	18:07	59 ° 13.013 N	01 ° 18.055 W		Water: 0 m
A-1-2	15.06.2015	22:04	59 ° 29.953 N	02 ° 11.362 W		Aerosol nets: finishing
3332	16.06.2015	11:35	59 ° 30.031 N	06 ° 00.010 W		Water: 0, 20, 45, 130 m
3338	17.06.2015	10:40	59 ° 29.990 N	10 ° 00.007 W		Water: 0 m
3340	17.06.2015	20:40	59 ° 30.053 N	11 ° 19.597 W		Water: 0 m
3342	18.06.2015	8:23	59 ° 30.244 N	12 ° 59.331 W		Water: 0 m
3344	18.06.2015	19:08	59 ° 29.973 N	14 ° 59.894 W		Water: 0 m
3348	19.06.2015	14:18	59 ° 30.024 N	17 ° 59.947 W	2182	GS
		15:00				Water: 0, 35, 80, 450, 730, 2130, 2180 m
		18:57	59 ° 30.020 N	17 ° 59.972 W		MS-1
3352	20.06.2015	14:39	59 ° 30.134 N	20 ° 37.771 W	2821	GS
						Water: 0, 20, 33, 60, 1080, 2808, 2860 m
3359	21.06.2015	21:40	59 ° 29.965 N	24 ° 40.841 W	2515	GS
						Water: 0, 28, 60, 200, 618, 2489, 2541 m
	22.06.2015	0:12	59 ° 29.885 N	24 ° 42.105 W	2517	GC
		2:36	59 ° 30.301 N	24 ° 42.962 W	2517	MS-2
3365	22.06.2015	18:43	59 ° 30.013 N	26 ° 39.851 W		Water: 0 m
3369	23.06.2015	10:08	59 ° 29.991 N	29 ° 19.884 W		Water: 0 m
3372	23.06.2015	18:13	59 ° 29.987 N	30 ° 40.034 W		Water: 0 m
3378	24.06.2015	13:26	59 ° 29.977 N	32 ° 50.533 W	2175	GS
					2228	Water: 0, 30, 70, 450, 800, 2187, 2222 m
		15:49	59 ° 30.256 N	32 ° 50.546 W	2192	GC
		17:37	59 ° 30.267 N	32 ° 50.563 W	2192	MS-3
3383	25.06.2015	14:57	59 ° 28.945 N	36 ° 08.247 W	3083	GS
						Water: 0, 20, 70, 120, 1300, 3080, 3130 m
		18:03	59 ° 27.637 N	36 ° 09.998 W	3084	GS
3387	26.06.2015	10:58	59 ° 29.902 N	38 ° 39.980 W		Water: 0 m
3392	27.06.2015	7:28	59 ° 33.910 N	41 ° 00.140 W	2394	Water: 0, 30, 60, 2000, 2200, 2426 m
3410	28.06.2015	8:56	59 ° 56.130 N	42 ° 48.350 W		Water: 0 m
3415	29.06.2015	16:38	55 ° 34.313 N	46 ° 12.559 W	2985	Water: 0, 35, 60, 100, 2835, 2935, 2980 m
		18:10	55 ° 34.252 N	46 ° 12.695 W	2985	GS
		19:24	55 ° 34.221 N	46 ° 12.656 W	2985	GC
A-2-1	29.06.2015	22:32	55 ° 02.319 N	46 ° 18.555 W		Aerosol nets: beginning
P-5	30.06.2015	9:16	52 ° 34.044 N	46 ° 46.452 W		Water: 0 m
A-2-2	01.07.2015	10:09	46 ° 58.947 N	47 ° 43.408 W		Aerosol nets: finishing

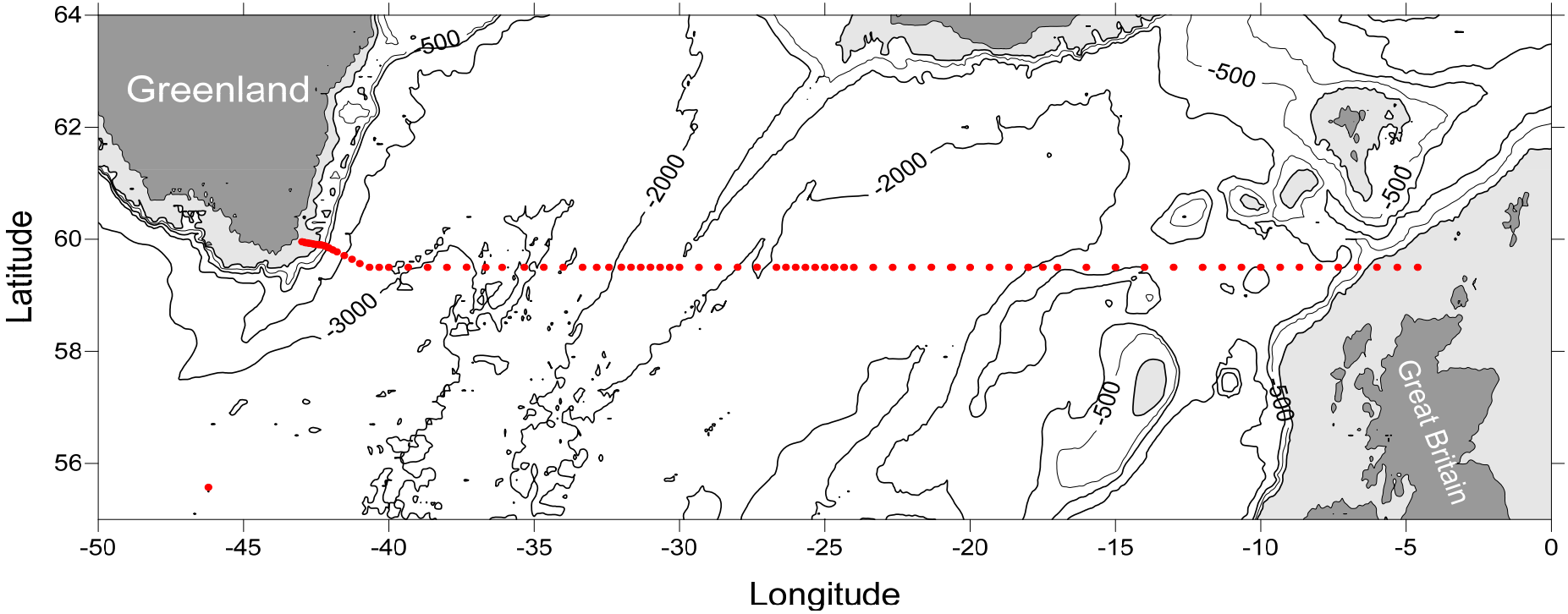

Fig. 1 Station locations (red circles). The shelf area with depth less than 200 m is shaded.

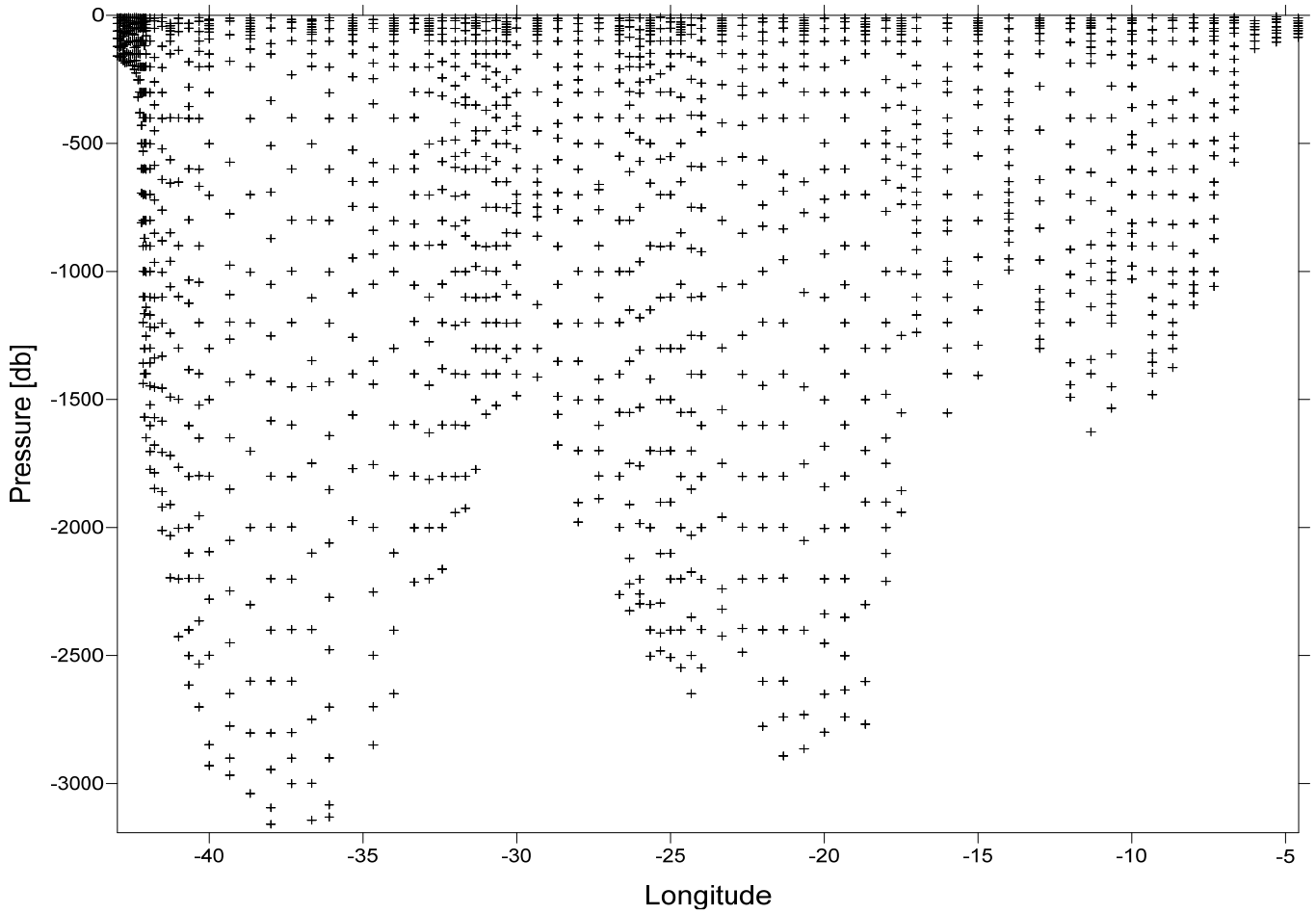

Figure 2. Vertical distribution of samples along the 59.5 section.

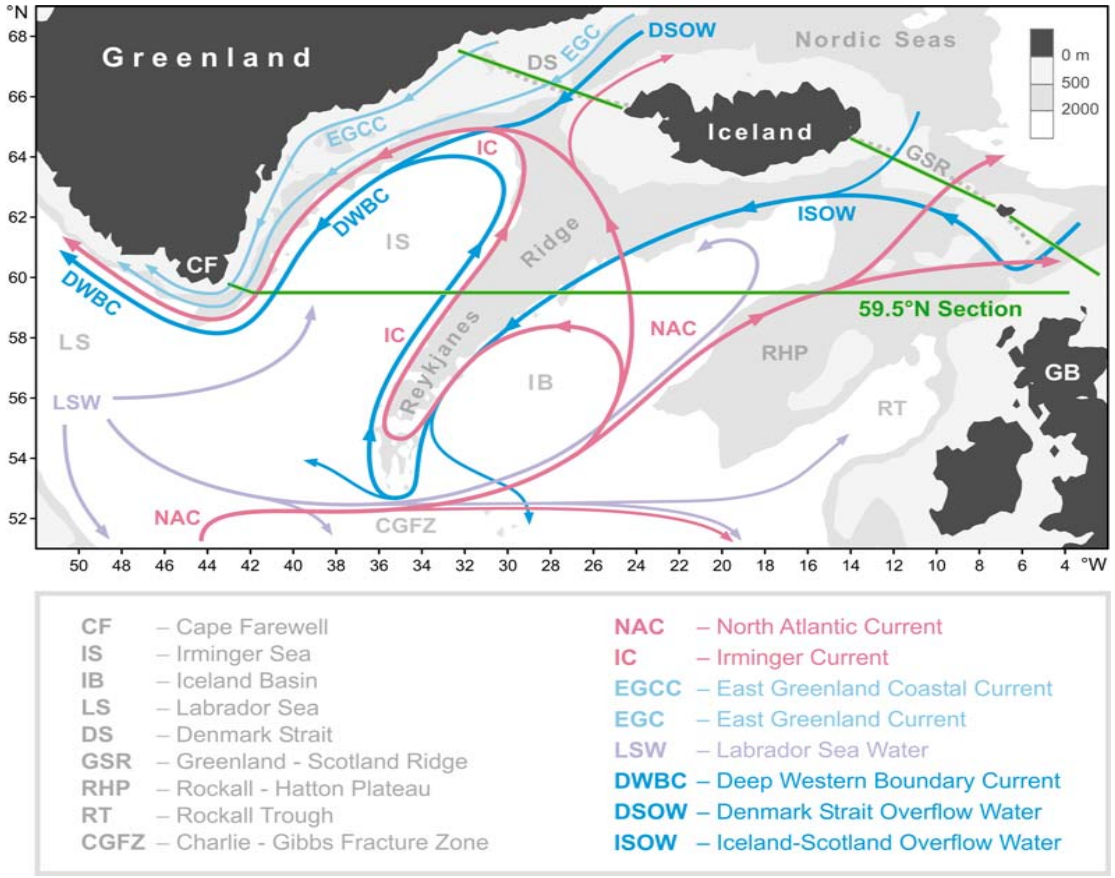

Figure 3. Schematic diagram of the large-scale circulation in the northern North Atlantic compiled from [Schmitz and McCartney, 1993; Schott and Brandt, 2007; Sutherland and Pickart, 2008; Lherminier et al., 2010]. Abbreviations for the main topographic features, currents and water masses are explained in the legend. The nominal locations of the 59.5°N hydrographic section (1997 – present) and sections across the straits between Greenland, Iceland, Faeroe and Shetland Islands (2011 – present) are shown with the solid green lines.

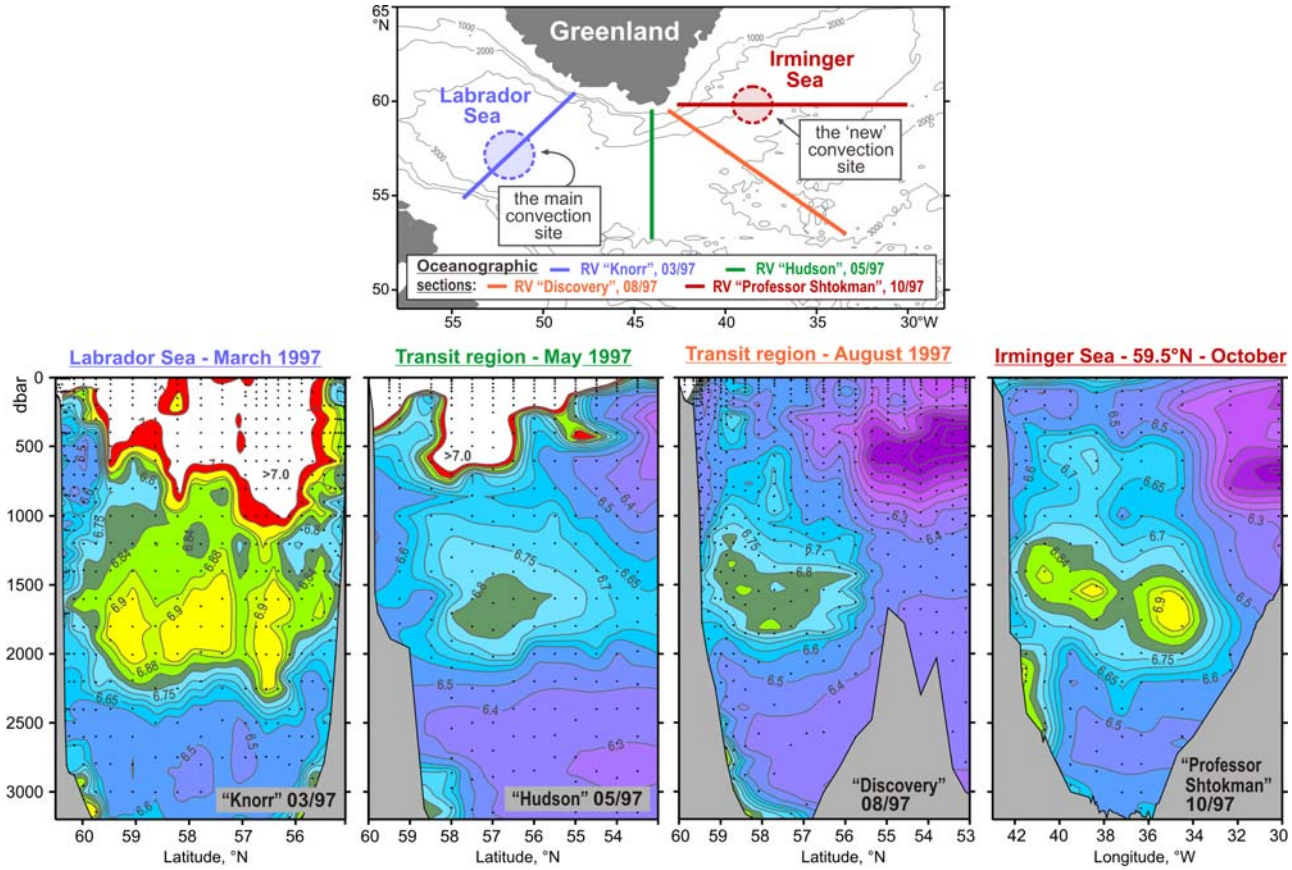

Figure 4. Oxygen concentrations (ml/l) in the water column (lower panel) as observed in March–October 1997 in four hydrographic sections (upper panel) ending nearby the southern tip of Greenland. A separate oxygen maximum in the LSW layer (1000–2000 m) in the Irminger Sea at 59.5°N strongly implies local convective renewal of LSW before 1997. Adapted from [Falina et al., 2007].

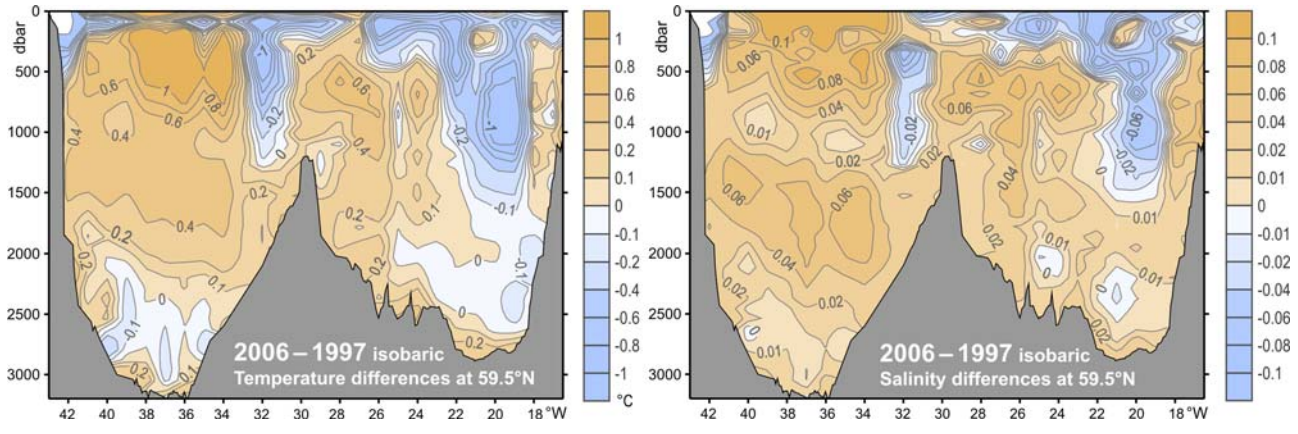

Figure 5. Warming and salinification in the northern North Atlantic between the mid-1990s and mid-2000s, as observed at 59.5°N. The figure shows the 2006–1997 temperature (°C, left) and salinity (right) differences on isobaric surfaces in the Irminger Sea and Iceland Basin. Adapted from [Sarafanov et al., 2007].

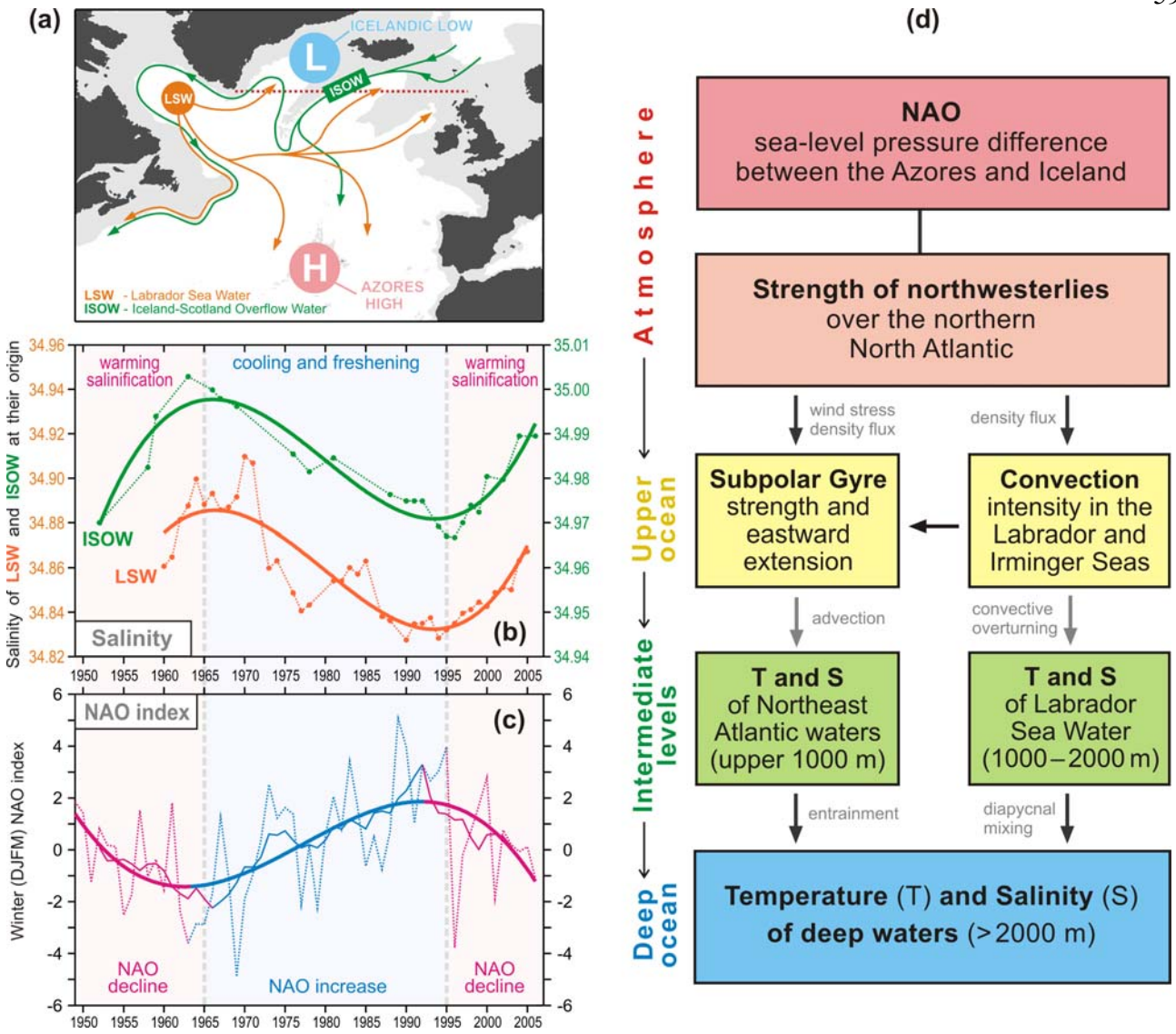

Figure 6. Coherence of the decadal salinity changes (1950s – 2000s) of the intermediate (LSW) and deep (ISOW) waters in the northern North Atlantic and their link to the North Atlantic Oscillation (NAO) index. **(a)** Schematic representation of the LSW and ISOW pathways and locations of the Icelandic Low (L) and Azores High (H) centers constituting the NAO dipole pattern. The red dotted line indicates the 59.5°N transatlantic section. **(b)** Salinity time series for LSW in the Labrador Sea [Yashayaev, 2007] and ISOW in the Iceland basin [Boessenkool et al., 2007; Sarafanov et al., 2007] overlaid by the third order polynomial fits. **(c)** Time series of the winter NAO index, after [Hurrell, 1995], overlaid by 7-year running mean and third order polynomial fit. **(d)** Mechanism of the NAO effect on the decadal changes in temperature (T) and salinity (S) of the northern North Atlantic intermediate and deep waters. Positive / negative links shown with the dark / light grey arrows mean that changes in 'causative' and 'consequential' characteristics have the same / opposite sign(s). The overall effect of the NAO on T and S of the in the water column is negative: persistent NAO decline leads to warming and salinification of the water masses and vice versa, as shown in (b) and (c). Adapted from [Sarafanov, 2009].

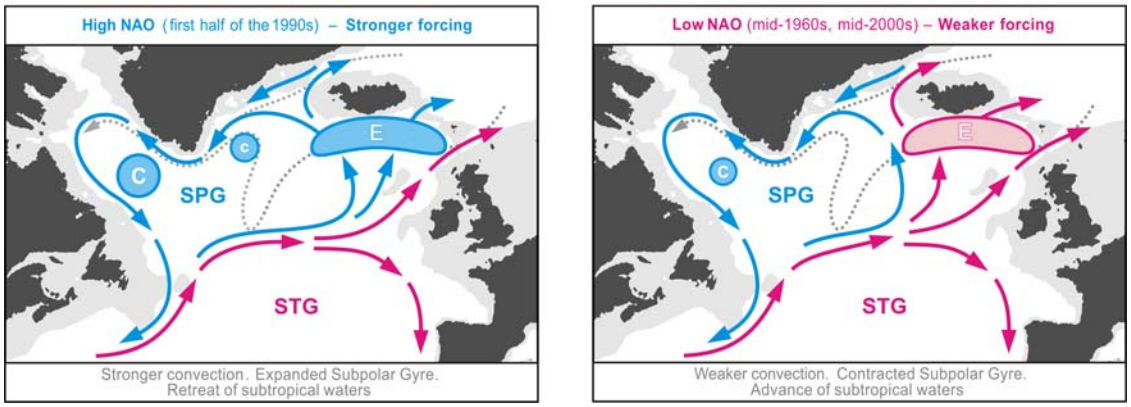

Figure 7. Schematic representation of the upper-ocean circulation and convection intensity in the northern North Atlantic under high (left) and low (right) NAO conditions. Blue (magenta) solid arrows indicate the upper-ocean flows with higher fraction of colder fresher subpolar (warmer saltier subtropical) waters. The main pathways of the Nordic overflow-derived deep waters are shown with the dotted curves. "C" and "E" symbols are used to denote, respectively, the deep convection sites and the domain, where the Atlantic waters are entrained into ISOW. Larger (smaller) circles indicate stronger (weaker) convection. SPG and STG – the subpolar and subtropical gyres, respectively. Adapted from [Sarafanov, 2009].

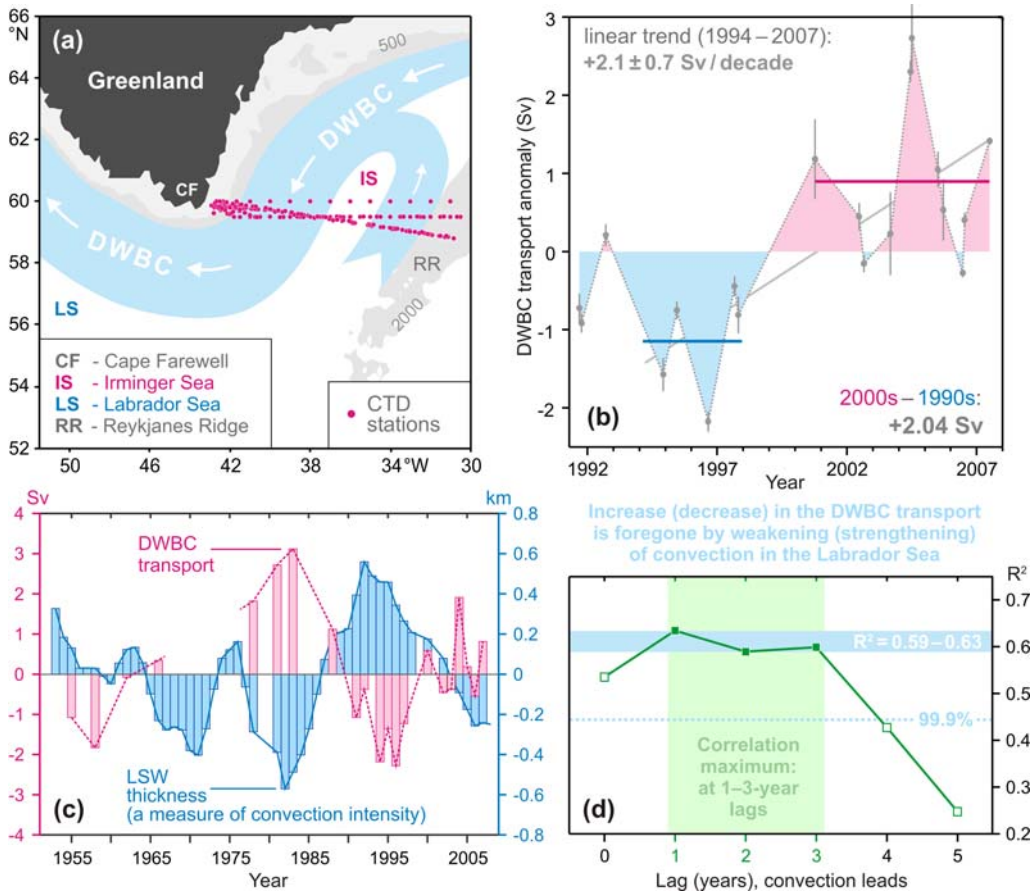

Figure 8. The Deep Western Boundary Current (DWBC) transport variability and its link to the convection intensity in the Labrador Sea. **(a)** Locations of the hydrographic sections (1991–2007) and schematic of the deep water circulation in the Irminger Sea. **(b)** The DWBC transport anomalies at Cape Farewell in 1991–2007, 1 Sv = 10^6 m^3 s^{-1}. The 1994–1997 and 2000–2007 mean anomalies and the 1994–2007 linear trend are shown. **(c)** Anomalies of the DWBC transport at Cape Farewell and the Labrador Sea Water (LSW) thickness in the Labrador Sea in the 1950s–2000s. **(d)** Correlation coefficient (R^2) for the two times series shown in **(c)** at the 0–5-year lag, the LSW thickness leads. The correlation maximum is achieved at the 1–3-year lag. The DWBC transport anomalies in the southern Irminger Sea are foregone by the convection intensity anomalies in the Labrador Sea. Adapted from [Sarafanov et al., 2009].

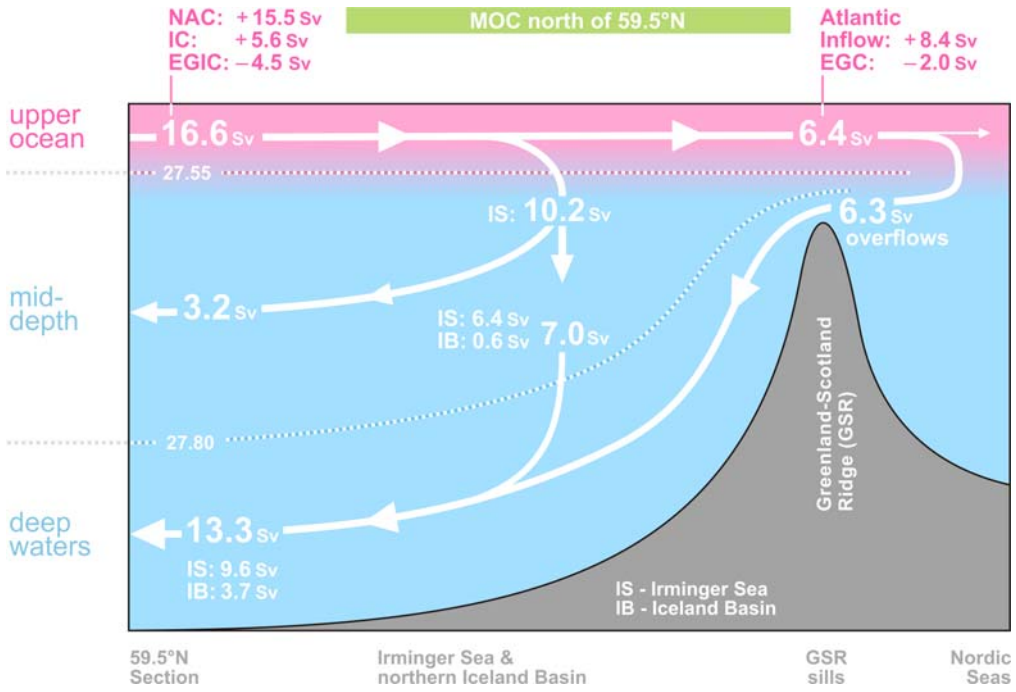

Figure 9. Schematic diagram of the Meridional Overturning Circulation (MOC) at the northern periphery of the Atlantic Ocean, northeast of Cape Farewell. The dotted lines refer to the σ_0 isopycnals 27.55 and 27.80. The arrows denote the integral meridional and diapycnal volume fluxes. Where the signs are specified, the positive (negative) transports are northward (southward). The NAC and EGIC transports in the upper layer ($\sigma_0 < 27.55$) at 59.5°N are the throughputs accounting for the recirculations. EGIC – the East Greenland / Irminger Current – refers to the upper part of the Western Boundary Current. Other abbreviations are explained in the legend to **Figure 3**. Adapted from [Sarafanov et al., 2012].

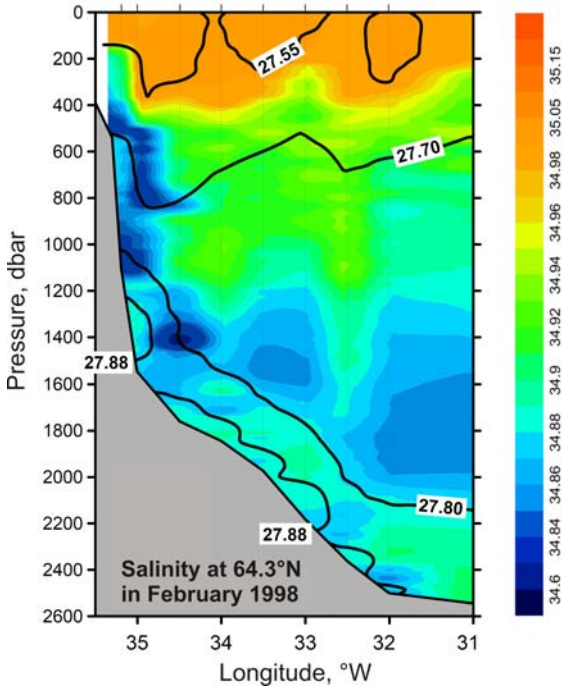

Figure 10. Salinity observed in the northwestern Irminger Sea at 64.3°N in February 1998. The σ_0 isopycnals 27.55, 27.70, 27.80 and 27.88 are plotted as the thick black lines; the station locations are marked with the ticks on the top axis. The plot shows fresh dense waters descending (cascading) down the continental slope of Greenland down to the LSW layer ($27.70 < \sigma_0 < 27.80$) and the layer of the Nordic Seas overflow-derived deep waters ($\sigma_0 > 27.80$). Adapted from [Falina et al., 2012].

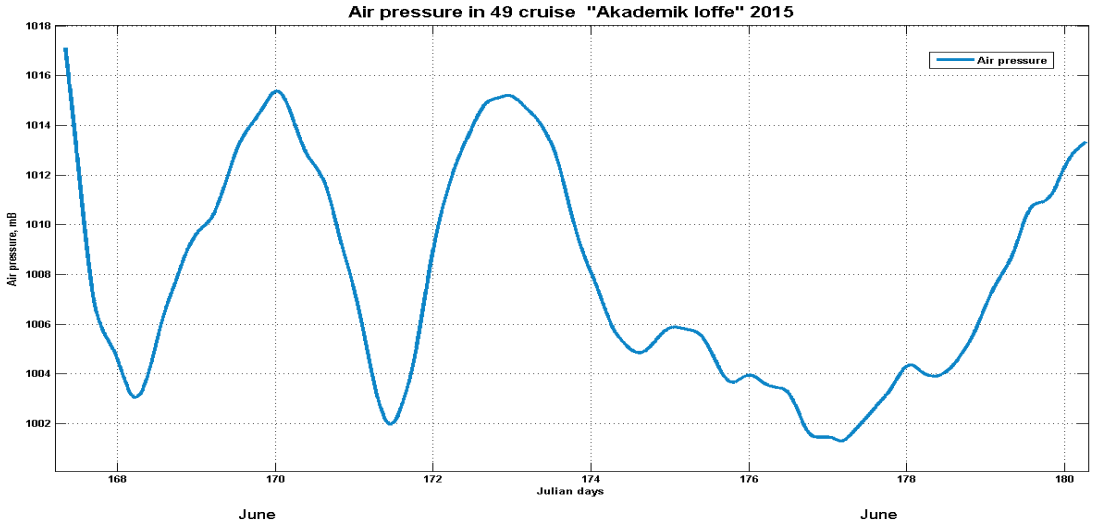

Figure 11. One-hour averaged atmospheric pressure (mb) measured during 49 cruise of Akademik Ioffe.

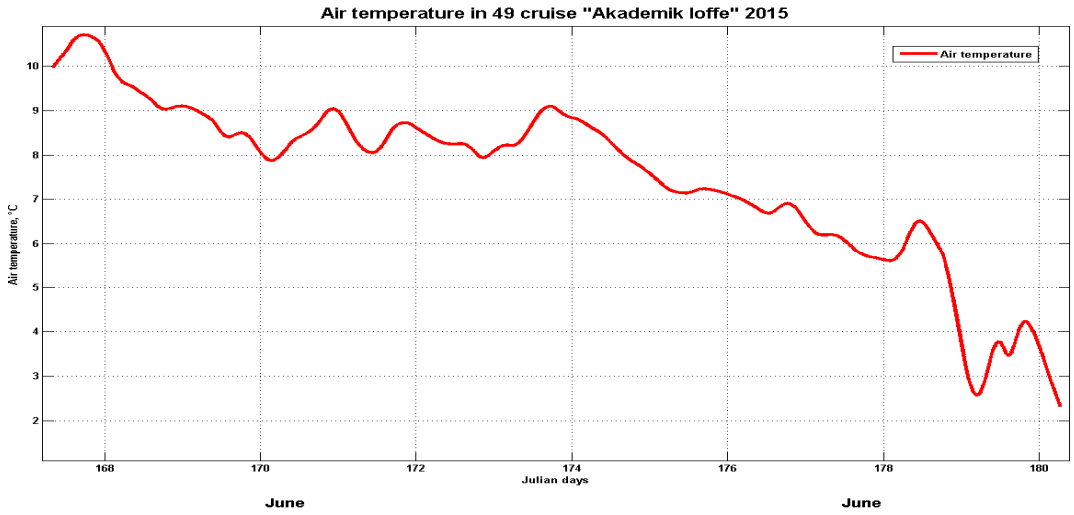

Figure 12. One-hour air temperature (°C) measured during 49 cruise of Akademik Ioffe.

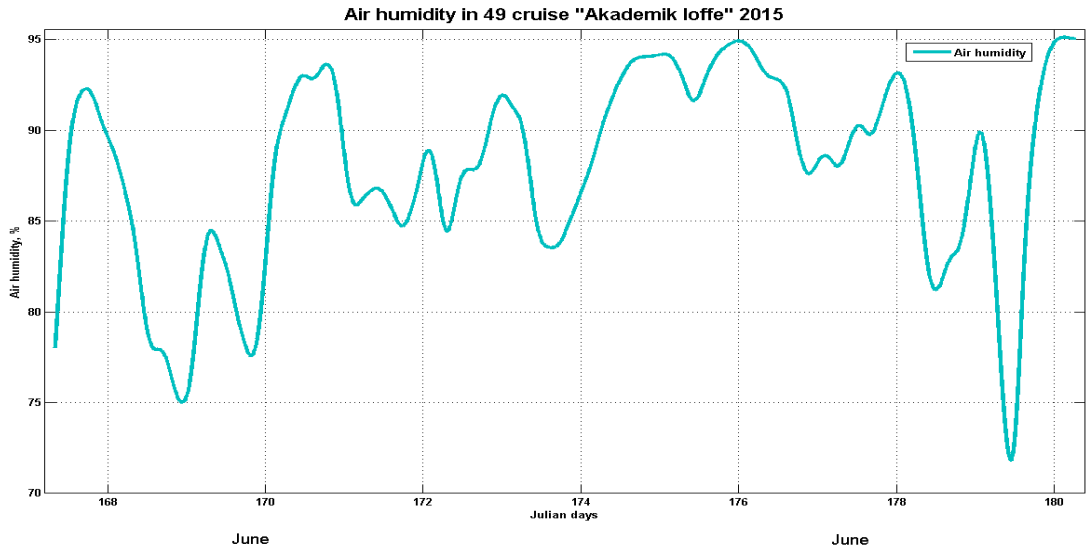

Figure 13. One-hour relative humidity (%) measured during 49 cruise of Akademik Ioffe.

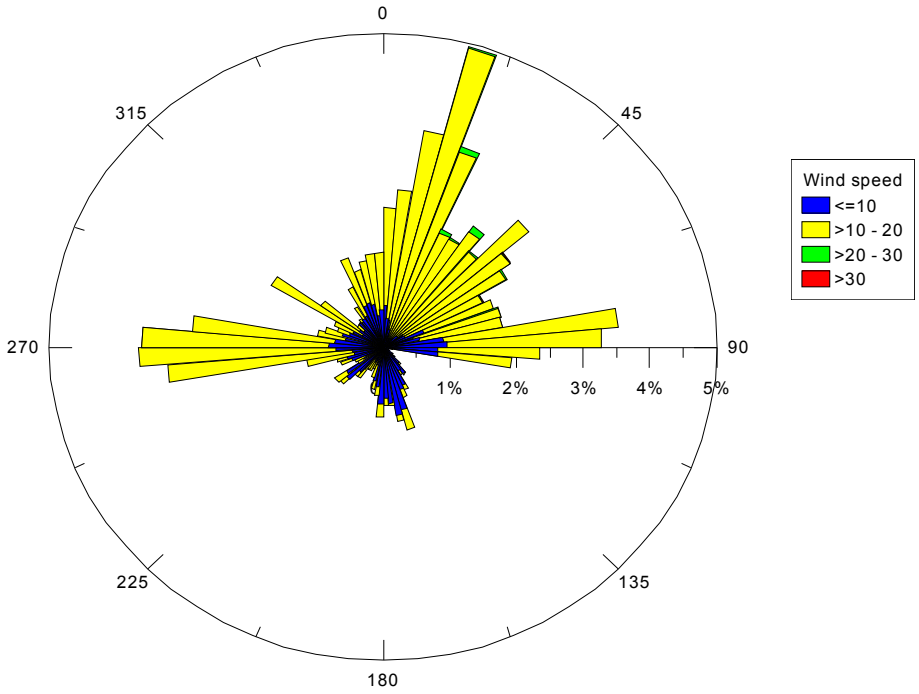

Figure 14. Wind speed and direction statistics during 49 cruise Akademik Ioffe.

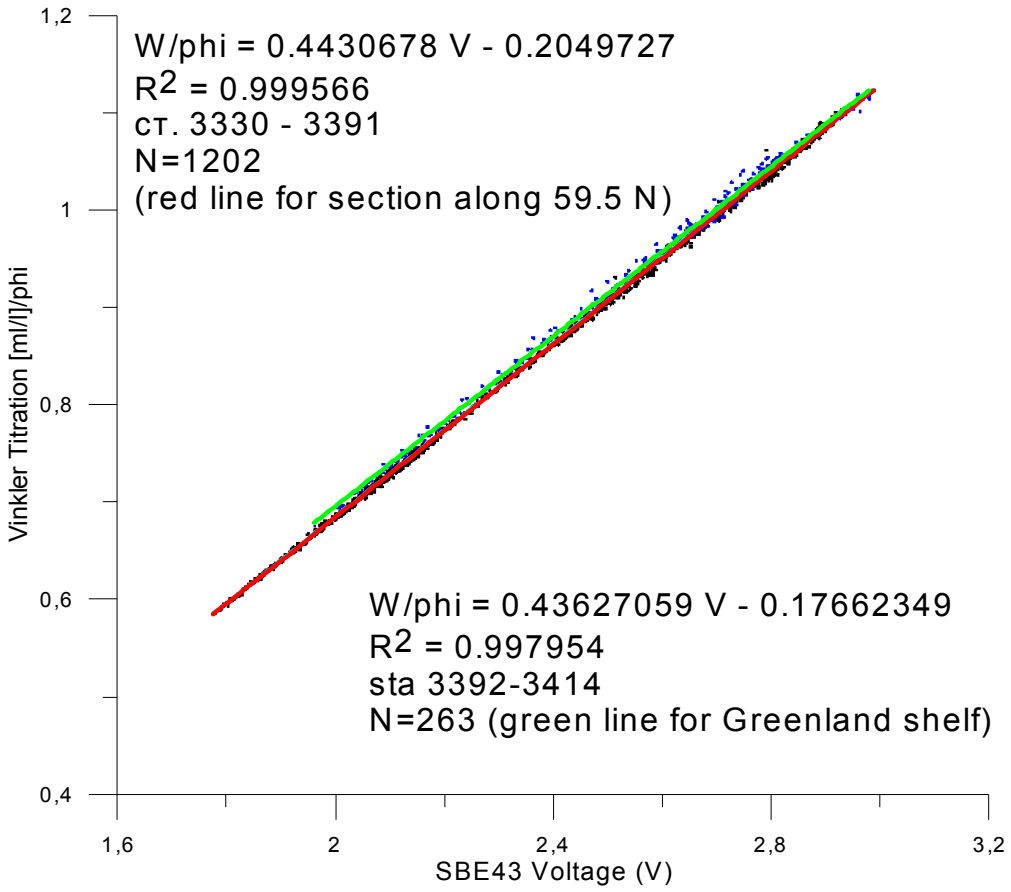

Figure 15. Regression line for Winkler oxygen divided by φ versus SBE 43 output voltage for the 59.5 section (red line). Oxygen data collected at the East Greenland shelf is regressed separately (blue dots, green line).

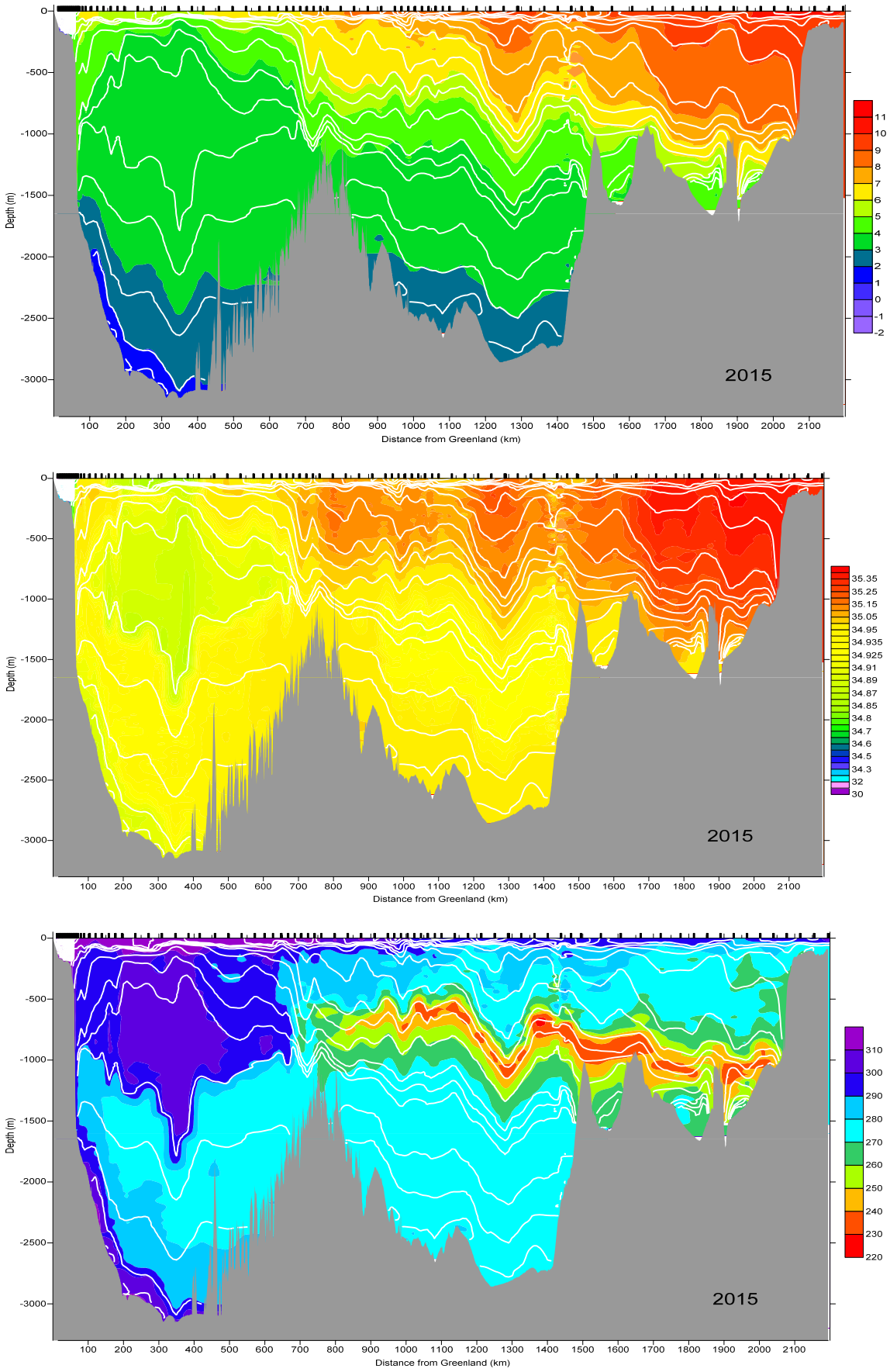

Figure 16 The vertical distribution of (a) potential temperature (°C) and (b) salinity and (c) CTD dissolved oxygen (µmol/kg) along 59.5 N in 16-29 June 2015. Potential density is shown by white lines. Station position is shown by vertical marks.

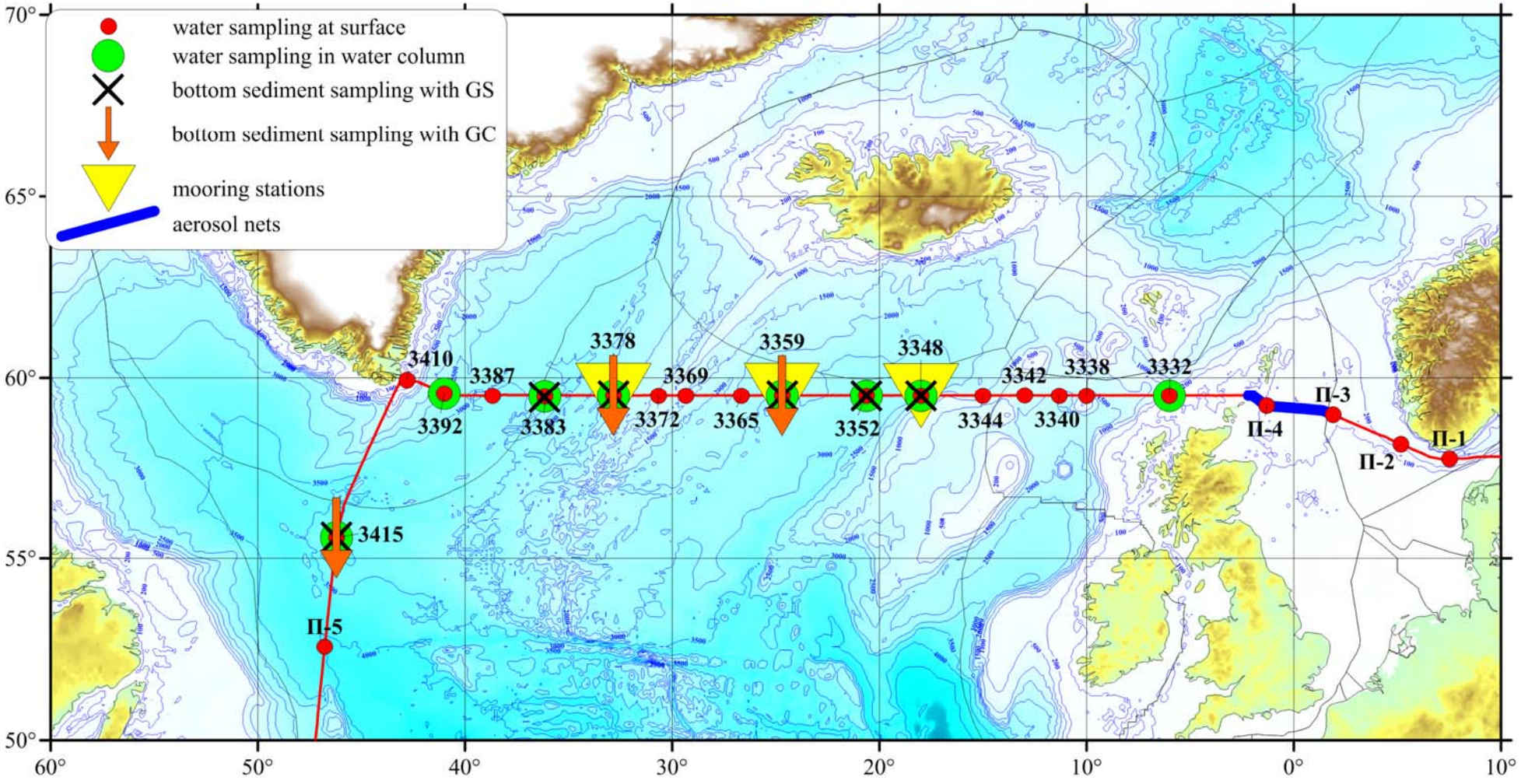

Figure 17. Chart of the geological stations in 49 cruise of RV Akademik Ioffe.

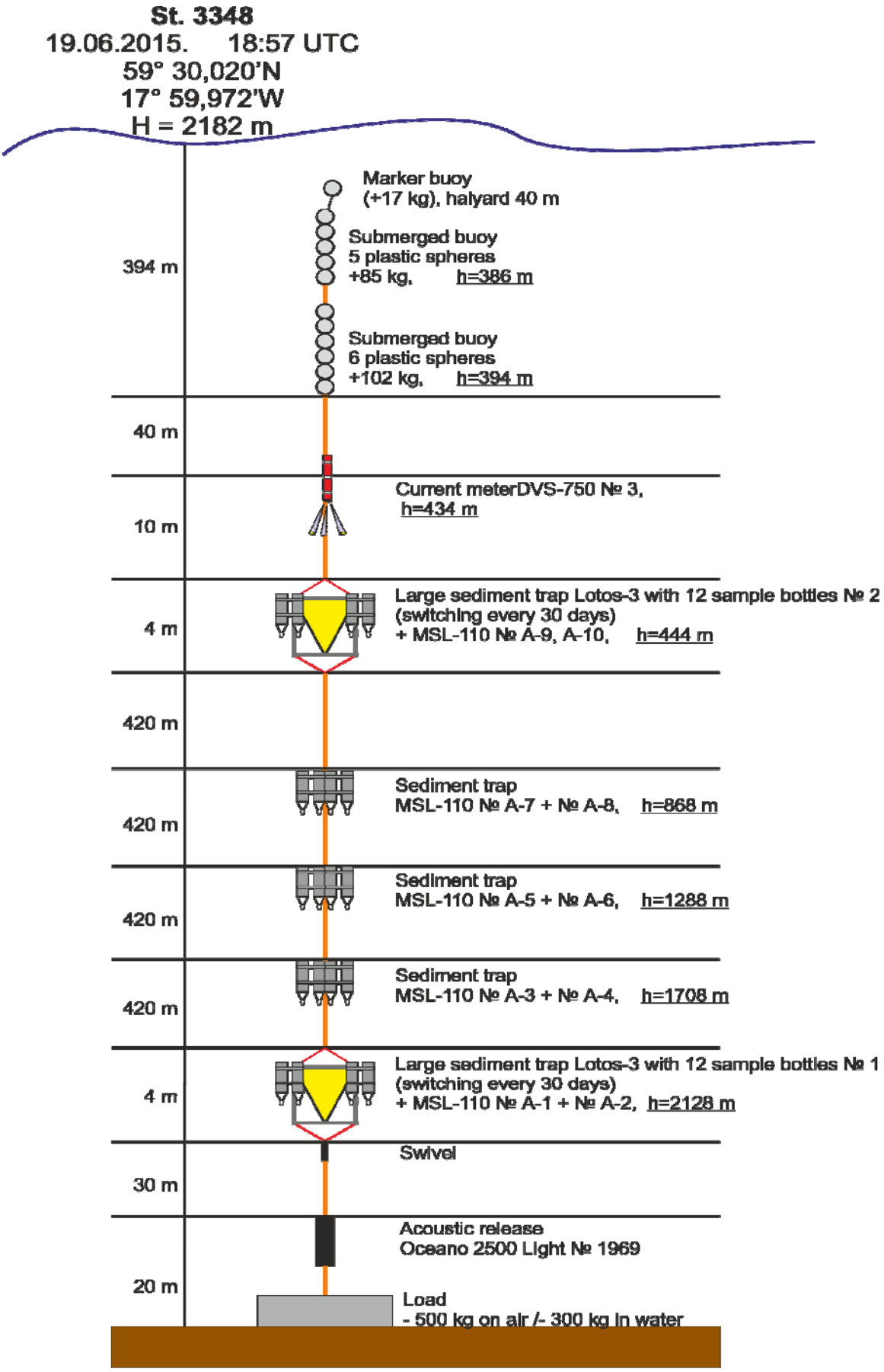

Figure 18. Mooring composition at sta 3348.

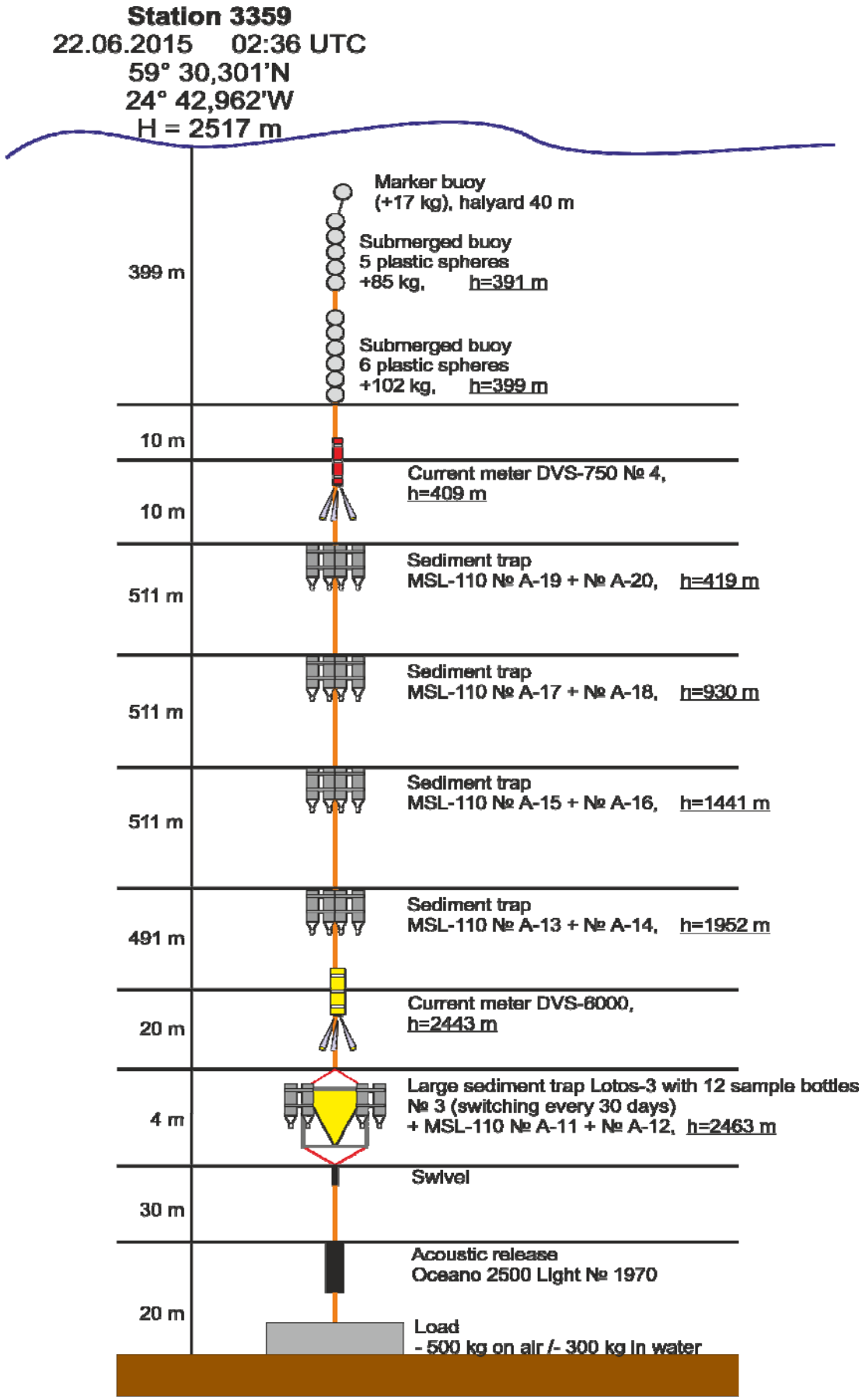

Figure 19. Mooring composition at sta 3359.

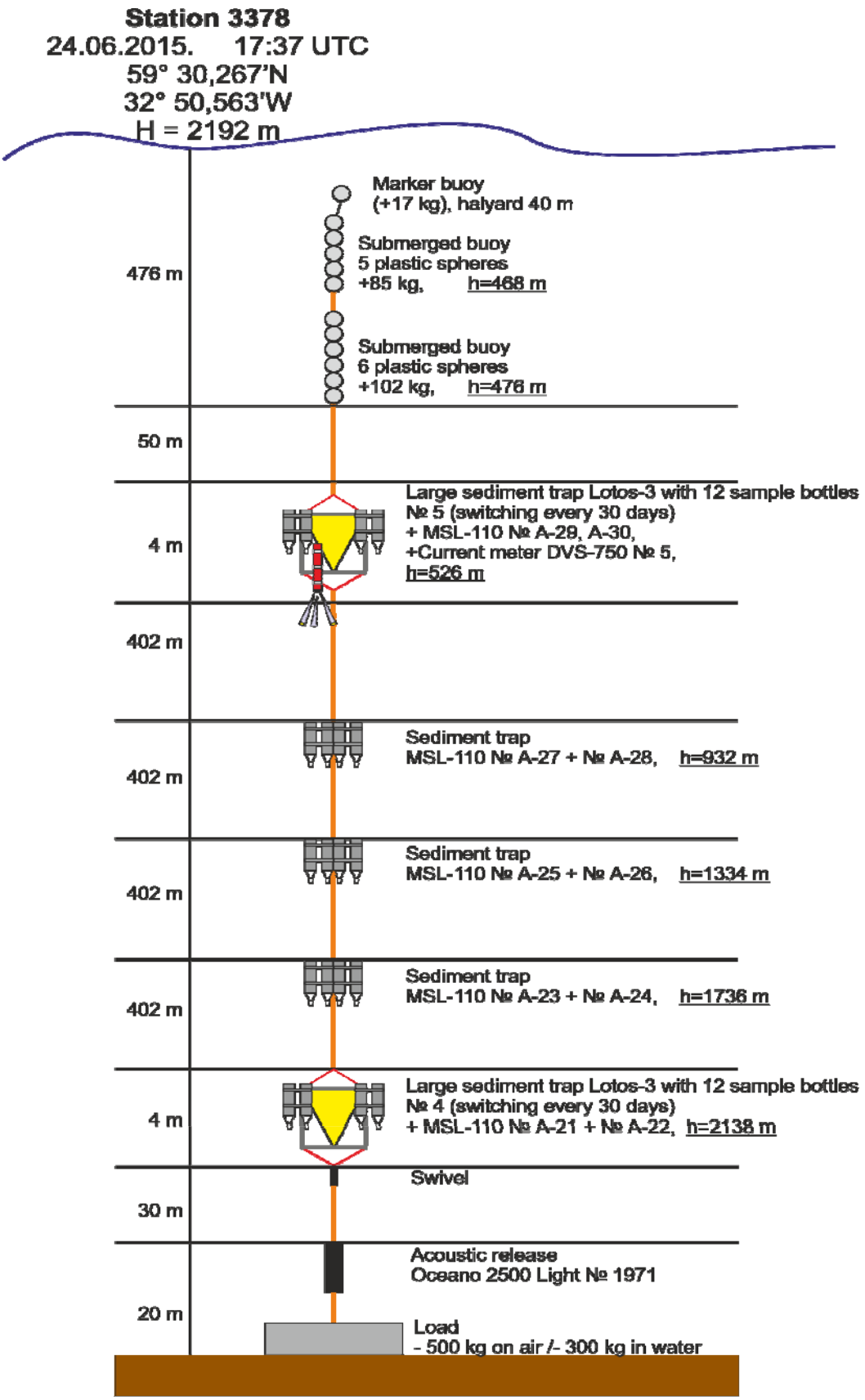

Figure 20. Mooring composition at sta 3378.